2010

Comprehensive study of parameters for volumetric modulated arc therapy (VMAT) treatment planning

Catharine Elizabeth Talbert
Louisiana State University and Agricultural and Mechanical College

COMPREHENSIVE STUDY OF PARAMETERS FOR VOLUMETRIC MODULATED ARC THERAPY (VMAT) TREATMENT PLANNING

A Thesis
Submitted to the Graduate Faculty of the
Louisiana State University and
Agricultural and Mechanical College
in partial fulfillment of the
requirements for the degree of
Master of Science

in

The Department of Physics and Astronomy

by
Catharine Elizabeth Talbert
B.A., Austin College, 2007
December, 2010

ACKNOWLEDGEMENTS

This work was supported in part by the Louisiana Board of Regents. I would like to thank Mary Bird Perkins Cancer Center, (Baton Rouge, LA) for providing the physical resources necessary to complete this project.

I would also like to acknowledge my advisor, Dr. Jonas Fontenot, for all the time and effort he put into this project and for helping me become a better writer, researcher, presenter, and critical thinker. I cannot thank him enough for continuously counseling me and giving me the confidence and motivation I needed to succeed. I would also like to thank my advisory committee: Dr. Kenneth Hogstrom, Dr. John Gibbons, Dr. Brent Parker, Dr. Maurice King, and Dr. Jim Matthews. Their wisdom, guidance, and constructive notes on my project were essential to the success of my project and were much appreciated.

I would like to thank my fellow students in the medical physics program, both current and previous, for their support, friendship, and comradery throughout the duration of the program. I would also like to thank the instructors and mentors who have guided me and helped me grow academically, intellectually, professionally and personally: Dr. Kip Matthews , Dr. Polad Shikahliev, Dr. Erno Sajo, Dr. Larry Robinson, Dr. Don Salisbury, and Dr . Karann Durland.

I would like to thank my family for always believing in me and pushing me to succeed in all my endeavors. I would not have succeeded without my parents' love and support and my brothers' constant playful criticism. I am the product of a loving, supportive home, and I am eternally grateful for the opportunities that have been presented to me.

Finally, I would like to thank my husband, Michael, for his love, encouragement, and support. Being married to a graduate student is not an easy task, but he plays the part with grace and patience that I will always admire and appreciate.

TABLE OF CONTENTS

ABSTRACT

Volumetric modulated arc therapy (VMAT) is a rotational IMRT technique that uses a radiotherapy linear accelerator gantry with a dynamic MLC, variable dose rate, and variable gantry speed. These new degrees of freedom of VMAT delivery introduced complexities for treatment planning, and Pinnacle^3 SmartArc treatment module was recently developed as a solution. However, it was unclear how varying each SmartArc parameter affected the resulting plan quality. The purpose of this study was to systematically examine all planning parameters and quantify the effect of varying each on the quality of a reference plan.

Parameters were separated into two categories: commissioning parameters and planning parameters. Commissioning parameters were those available to the user during the machine commissioning process in Pinnacle, *i.e.* dose rate, gantry speed, MLC size, and MLC speed. Planning parameters were those available to the user during routine treatment planning, *i.e.* beam energy, collimator angle, arc length, and final gantry spacing. A "baseline" set of commissioning and planning parameters was created that provided clinically acceptable plans for a cylindrical phantom case, simple prostate case, and complex (multi-target) prostate case. Each parameter was independently varied while keeping all other parameters set to the baseline values. The resulting change in each plan was evaluated using dose volume histograms, dose homogeneity indices (DHI), conformity indices (CI) and normal tissue dose metrics.

The DHI and CI for the phantom and simple prostate cases varied by less than 0.02 from the baseline values for most parameters. The DHI and CI for the complex prostate case varied by more than 0.02 from the baseline values for most parameters. The dose to normal tissues changed by less than 3% as parameters were varied for the simple prostate case and more than 3% as parameters were varied for the complex prostate case.

Most SmartArc parameters had little effect on DHI, CI, and normal tissue sparing for the phantom and simple prostate treatment geometries, but showed significant variations for the complex prostate case. We conclude that SmartArc optimization is largely user-independent and hardware-independent for non-complex prostate treatment geometries. However, certain parameters (especially planning parameters) create a significant change in resulting plan quality for complex prostate treatment geometries.

1 INTRODUCTION

1.1 Background and Significance

1.1.1 History and Development of VMAT

Intensity modulated arc therapy (IMRT) is a radiation treatment modality that provides accurate, reliable, and highly conformal dose to a planning target volume (Khan 2003). Several techniques of delivering IMRT have been established: static-gantry techniques, such as fixed-beam IMRT; and rotational-gantry techniques, such as helical tomotherapy (Mackie *et al.* 1993; Bortfeld and Webb 2009). Fixed-beam IMRT has been shown to provide better dose conformality and normal tissue sparing than 3-D conformal treatments (Staffurth 2010), but it is still limited by only using a finite number of beams for delivery. Helical tomotherapy also provides highly conformal dose distributions, but requires specialized delivery hardware and treatment planning software. Both fixed-beam IMRT (except for compensator-based IMRT) and helical tomotherapy increase treatment delivery time compared to 3-D conformal treatments, which could lead to greater problems in dose accuracy due to intra-fractional motion.

The idea of using a traditional linear accelerator gantry for a rotational IMRT treatment was first suggested by Yu et al. in 1995 as an alternative to tomotherapy, which necessitated specialized equipment and struggled with abutment problems between treatment slices at that time. Yu's alternative was called intensity modulated arc therapy (IMAT) and utilized a large field size, traditional linear accelerator, continuous gantry rotation, and dynamic MLC. To create an intensity distribution, IMAT was delivered in multiple overlapping arcs. Each arc delivered only one level of intensity; therefore multiple arcs were required for multiple levels of intensity. The two-dimensional intensity distribution at each angle was a composition of multiple radiation fields of uniform intensity with different shapes and sizes. Shortly after IMAT

was proposed, helical tomotherapy was created, alleviating abutment problems without the necessity of developing new software for optimization and delivery of IMAT. As such, IMAT was never used in mainstream clinical practice.

Developments in rotational delivery capabilities of traditional linear accelerators in the last few years, specifically variable dose rate and variable gantry speed, have sparked a new interest in rotational IMRT delivery and IMAT (Bortfeld and Webb 2009). Volumetric modulated arc therapy (VMAT) has been developed using the basic principles of IMAT, coupled with these new machine capabilities. During a VMAT treatment, MLC leaves dynamically shape the beam to treat the entire volume of the planning target volume (PTV) with every rotation, and the dose rate and/or gantry rotation speed is continuously varied as the gantry of the linear accelerator rotates around the patient. Because of the ability of the linear accelerator to vary dose rate and gantry speed during rotation, it is no longer necessary to use multiple overlapping arcs to create modulated intensity, and an entire fraction of treatment can often be delivered in a single arc (Bortfeld and Webb 2009).

Both Elekta, Inc. (Stockholm, Sweeden) and Varian Medical Systems (Palo Alto, California) have developed VMAT capabilities on their traditional linear accelerators. Varian has named this new version of VMAT "RapidArc," while Elekta refers to it as "VMAT." In this study "VMAT" is used as a generic term for a dynamic arc IMRT treatment modality that uses dynamic MLC, variable dose rate, and variable gantry speed, and is not meant to be vendor-specific.

1.1.2 Technical Description of VMAT

Three key components of VMAT are rotational delivery, dynamic MLC, and variable dose rate and gantry speed. To describe these components, it is useful to compare and contrast

VMAT to both fixed-beam IMRT and tomotherapy. Although VMAT and tomotherapy are both rotational treatment modalities, their delivery methods are very different. Tomotherapy, meaning 'slice therapy,' uses a fan beam and ring gantry to treat one transverse slice of the PTV at a time (Mackie *et al.* 1993). In helical tomotherapy, much like helical computed tomography, the couch moves perpendicularly to the gantry plane while the gantry rotates around the patient, creating a spiral-treatment (Yang *et al.* 1997). With VMAT, however, the entire PTV is treated with every rotational pass of the gantry (Cao *et al.* 2007). This means VMAT has the potential to treat the entire PTV to the desired dose using a single arc (Otto 2008). In other words, tomotherapy can be considered a planar delivery technique, whereas VMAT is a volumetric

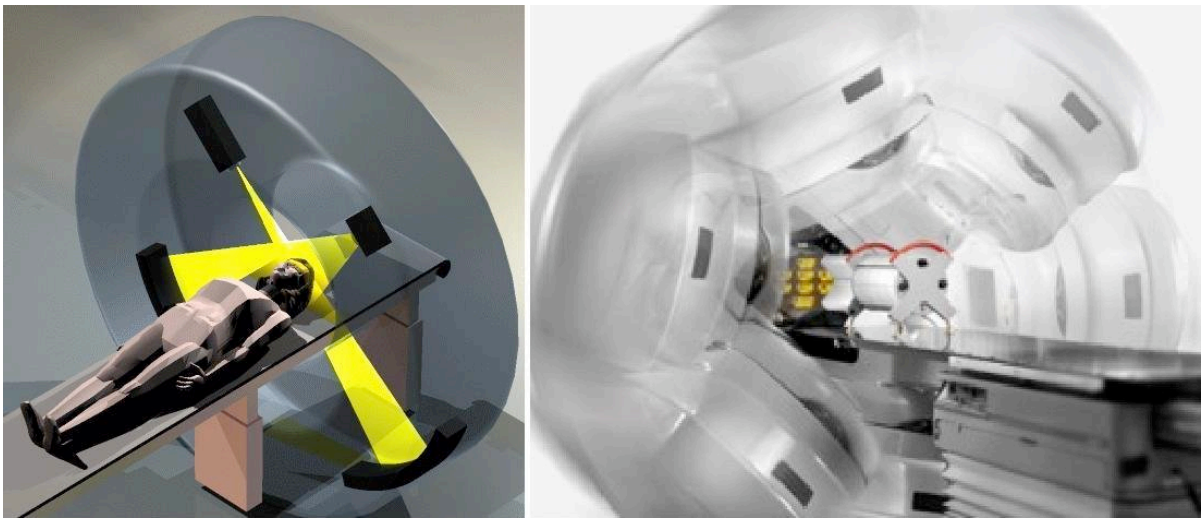

Figure 1-1. Tomotherapy slice delivery (left) vs. VMAT volumetric delivery (right).

delivery technique. A schematic of the difference in delivery is shown in Figure 1-1. Both gantries rotate around the patient, but the tomotherapy couch moves into the gantry to create a helical slice delivery while the VMAT couch remains stationary as the beam treats the entire PTV.

The next key component of VMAT treatments is the dynamic MLC. Treatment plans for fixed-beam IMRT are comprised of a finite number of beams at fixed angles around the patient.

In order to produce an optimized fluence pattern for each fixed beam, the MLC leaves move either dynamically (Svensson *et al.* 1994) or in a step-and-shoot fashion (Wu *et al.* 2001) across

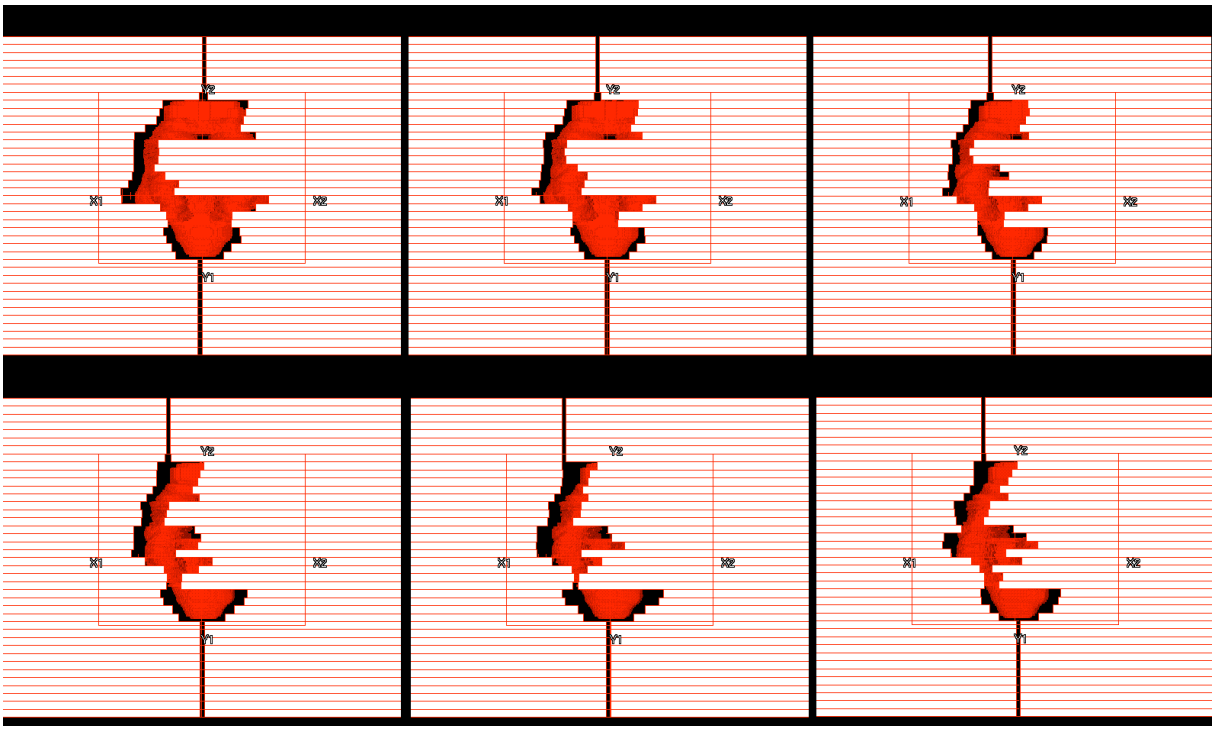

Figure 1-2. Sample MLC segments for VMAT delivery for 6 consecutive control points. MLC leaves (white) do not simply follow the shape of the PTV (red) as the gantry rotates around the patient.

the beam, creating several segments with different intensities to modulate the beam. Compensator-based IMRT does not use MLCs, but instead a tissue compensator is fabricated for every beam angle and attached to the machine before the beam is delivered. In tomotherapy treatments, beams are optimized for 51 arc segments in each slice, and the binary MLC leaves are either open or closed for some specific amount of time during the arc segment in order to modulate the beam (Mackie *et al.* 1993). For both fixed-beam IMRT and helical tomotherapy, the beam modulation is determined by the amount of time the leaves spend in each position. VMAT treatments must use a dynamic MLC because the beam is on during the entire treatment as the gantry rotates around the patient. For VMAT treatments, the MLC leaves move as a

function of gantry position, not time (Bortfeld and Webb 2009). The leaves reposition according to where the gantry is located in its rotation, and each angle of rotation sees only one segment shaped by the MLC. However, because the leaves do not simply conform to the shape of the PTV, VMAT can still be considered a form of IMRT, not 3-D conformal therapy. An example of MLC segment positions as the gantry travels around the arc is shown in figure 1-2. The leaves are used to modulate the intensity distribution.

Rotational delivery adds the flexibility of treating at every angle, which can be greatly advantageous for some treatment sites, but the limited MLC range of motion per gantry angle somewhat limits this flexibility (Otto 2008). Because the MLC leaves have a maximum speed, the distance they travel is limited by how slowly the gantry can rotate. Limited leaf motion and continuous beam delivery can quickly lead to unwanted dose to normal tissues. To obtain a sufficient intensity resolution without the necessity of using overlapping arcs (Yu 1995; Earl *et al.* 2003), the dose rate and/or gantry speed are varied throughout the VMAT treatment. This creates a direct modulation of beam output that is unique to VMAT delivery. During VMAT treatment, the beam output is changed according to gantry position, whereas intensity modulation in both tomotherapy and fixed-beam IMRT results from changing the beam-on time for each MLC segment. VMAT delivery combines varying leaf motion with varying dose rate and/or gantry rotation speed to modulate beam intensity.

1.1.3 Advantages and Disadvantages of VMAT

The most frequently-mentioned and advertised benefits of VMAT are decreased treatment time and increased monitor unit (MU) efficiency. If only a single arc is used, the beam-on time is reduced to the time it takes the gantry to rotate from the start angle to the stop angle position (including variations in gantry speed). This can accomplish a substantially shorter

overall treatment time than both helical tomotherapy and fixed-beam IMRT (Webb and McQuaid 2009). It has been shown that for prostate and head and neck treatment sites, VMAT plans with similar or better quality than fixed-beam IMRT could be delivered in less than 3 minutes, compared to 8-12 minutes for fixed-beam IMRT delivery (Bzdusek *et al.* 2009; Verbakel *et al.* 2009; Shaffer *et al.* 2009; Zhang *et al.* 2009). The shorter overall treatment time has been advertised to lead to greater patient compliance as well as greater throughput for the radiation treatment facility. Alternatively, shorter beam-on time may allow for use of more advanced image-guidance tools, such as on-board cone beam computed tomography that is now becoming widely available, without sacrificing overall treatment time.

VMAT also has much higher MU efficiency than other forms of IMRT delivery, with the exception of compensator-based IMRT. This means VMAT can treat the PTV to the same dose using fewer MU than fixed-beam IMRT and helical tomotherapy. Fixed-beam IMRT and tomotherapy keep the dose rate constant and change the amount of beam-on time for each MLC segment to modulate intensity. With these techniques, much of the beam is "wasted" for small fields. Because VMAT directly varies the dose rate of the beam to change the beam's intensity, it is much more efficient in terms of MUs than both tomotherapy and fixed-beam IMRT. Verbakel et al. found that VMAT reduced the number of monitor units used per fixed-beam IMRT treatment by 40 percent for head and neck geometries (2009). Bzdusek found MUs were decreased up to 23 percent for lung geometries, 13 percent for whole brain, and less than 10% for tonsil and prostate, where MU for one of three prostate cases actually increased 29 percent (2009). Also, photon x-ray beams with energy less than 10MV are typically used for IMRT because IMRT treatments require more MUs than conformal treatments, causing increased secondary radiation to normal tissues outside the radiation field due to leakage and scatter. For

energies greater than 10MV, neutron production from photon interactions in the machine head also increases with increasing MU (Reft *et al.* 2006). By requiring fewer MUs, VMAT can potentially allow for usage of higher energy photons with reduced risk of secondary cancers.

Disadvantages of VMAT include a limited beam size, which makes VMAT incapable of treating long PTVs (*e.g.* craniospinal cases) without abutment of two arcs. Also, multiple superimposed arcs may be required for VMAT to achieve comparable modulation and dose distributions to those achieved by Tomotherapy.

1.2 Optimization of VMAT

Along with the evolution of rotational delivery capabilities of the treatment machine, substantial changes in the optimization algorithms used for fixed-beam IMRT were necessary in order to make VMAT clinically possible. These included techniques for creating an effective 360 degree fluence map and the addition of several new optimization parameters. The optimization module used in this study was SmartArc, developed for the Pinnacle^3 treatment planning system (Philips Medical Systems, Andover, MA).

Though the beam treats in a continuous arc, there are a finite number of control points (CPs), or samples around the arc used for optimization and delivery. This produces a tradeoff between dose delivery accuracy and optimization computation time (Otto 2008); more CPs leads to better plan accuracy but longer computation time. Otto proposed implementing "progressive sampling" as a compromise. First, coarse sampling is used to create intensity maps for several angles around the arc, and then subsequent CPs are added in smaller degree increments to increase plan dosimetric accuracy. Figure 1-3 shows a diagram of progressive sampling.

Bzdusek *et al.* (2009) incorporated progressive sampling in their VMAT optimization solution for the SmartArc treatment planning module. First, an initial coarse sampling increment

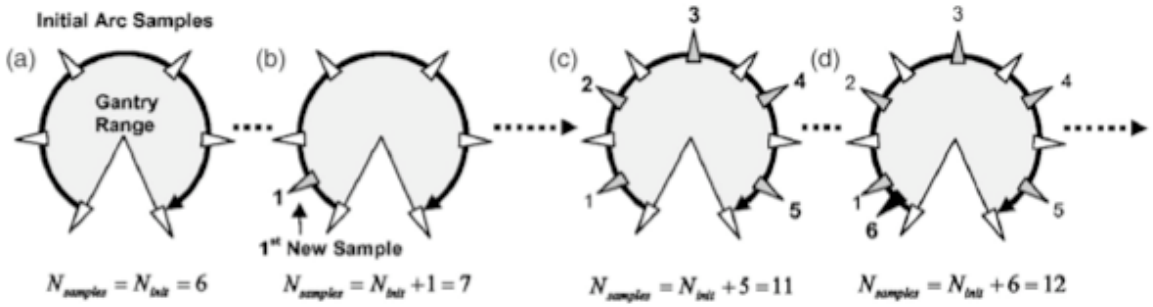

Figure 1-3. Diagram of progressive sampling. An initial coarse CP spacing is chosen (a) and intermediate CPs are added between existing CPs until desired CP frequency is reached (b-d). *Figure reprinted from Otto 2007*, Medical Physics, *Vol. 35 p 312*

of 24 degrees is used, and fluence maps are generated, optimized, and converted to leaf segments for these angles. Then, intermediate MLC segments are linearly interpolated between the coarse segments, creating a finer CP spacing (Bzdusek *et al.* 2009).

SmartArc optimization module is outlined in Figure 1-4. First, intensity maps are optimized every 24 degrees around the arc and converted to 2-4 different MLC segments. The

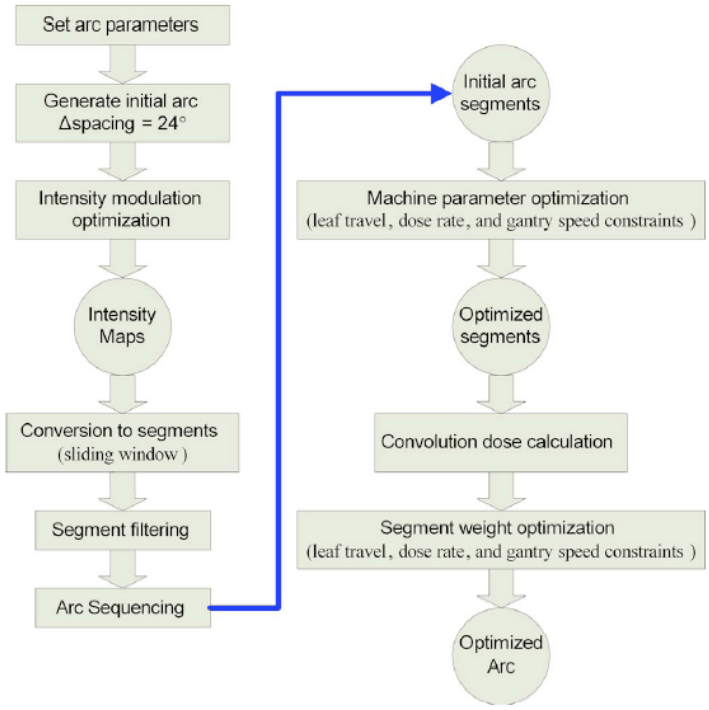

Figure 1-4. Outline of SmartArc optimization. *Figure reprinted from Bzdusek et al. 2009,* Medical Physics, *Vol. 36 p 2330*

two MLC segments that have the most open space are selected and redistributed 8 degrees above and below the point along the arc where the intensity map was initially created (every 24 degrees). The two segments with the most open space are selected in order to minimize leaf travel between CPs. The remaining MLC segments generated for that point are discarded. Additional MLC segments are then linearly interpolated to create the CP resolution, or final gantry spacing, selected by the user (2, 3, 4, or 6 degrees). Figure 1-5 shows the filtering, redistribution and sequencing of MLC segments.

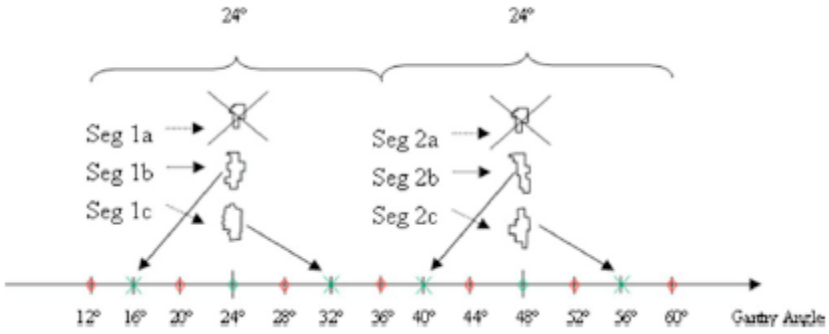

Figure 1-5. Diagram of MLC segment creation for SmartArc optimization. 2-4 segments are generated at the initial CP spacing (24º), then 2 are selected and redistributed (crosses) while the others are discarded. Additional MLC segments are interpolated between the initial segments (first blue circles, then red). *Figure reprinted from Bzdusek et al. 2009,* Medical Physics, *Vol. 36 p 2330*

After initial arc MLC segments have been interpolated, machine parameters are optimized, followed by a convolution dose calculation and segment weight optimization. Then the process is repeated until the number of iterations is reaches its limit. The result is that every 2, 3, 4, or 6 degrees, the treatment control system is given a new set of directions until it arrives at the next CP. The set of directions includes MLC configuration, leaf speed, dose rate and gantry rotation speed.

1.3 Motivation for Research

Clinical treatment planning requires commercialized software and tested protocols to accurately construct radiation therapy treatment plans that maximize the capabilities of available technology. While such tools have long been established for tomotherapy and fixed-beam IMRT, analogous tools for VMAT are still in the development stages. Recently a commercial utility, Phillips Pinnacle^3 SmartArc (described above), has been created to optimize VMAT treatments; however, the optimization process contains numerous parameters and options that have not yet been fully explored (Bzdusek *et al.* 2009). It is currently unknown how each of these parameters may be used to generate an optimal treatment plan for any particular treatment site.

The goal of this study was to systematically vary and examine new parameters introduced by VMAT (such as variable dose rate) and previously existing parameters (such as maximum gantry speed) that had potential to influence resulting VMAT plans. A comprehensive study of all parameters related to VMAT treatment planning is clinically relevant and useful for future treatment planning.

1.4 Hypothesis and Specific Aims

Our hypothesis was that a set of parameters for the Phillips Pinnacle^3 SmartArc treatment planning module could be determined that produce dynamic arc plans with

1) treatment times less than half that of corresponding fixed-beam IMRT plans, and

2) better than ±3% dose homogeneity in the PTV of a water phantom, ±5% dose homogeneity in the PTV of a simple prostate patient, and ±5% dose homogeneity in the primary PTV of a multi-target complex prostate patient

while maintaining sufficient sparing of critical structures.

Specific Aim 1: Determine a set of baseline parameters for planning VMAT treatment for a spherical PTV in a simple water-equivalent phantom, and then vary parameters systematically. The baseline plan was considered acceptable if it maintained ±3% dose homogeneity within the PTV. All parameters were kept identical to the baseline set except the parameter actively being studied.

Specific Aim 2: Determine a set of baseline parameters for planning VMAT treatment for a simple prostate patient, and then vary parameters systematically. A previously treated, simple prostate patient involving a single target was selected. The baseline plan was considered acceptable if it maintained ±5% dose homogeneity within the PTV and sufficiently spared surrounding critical structures.

Specific Aim 3: Determine a set of baseline parameters for planning VMAT treatment for a complex, multi-target prostate patient, and then vary parameters systematically. A previously treated, complex prostate patient involving multiple targets was selected. The baseline plan was considered acceptable if it maintained ±5% dose homogeneity within the PTV and sufficiently spared surrounding critical structures.

2 METHODS

To determine how optimization parameters affect resulting plan quality, parameters were varied and resulting plans evaluated for three treatment sites with increasing complexity. All cases were planned and optimized using Pinnacle[3] version 8.1y (Philips Medical Systems, Andover, MA). Version 8.1y was the first release of Pinnacle to include the SmartArc planning module, and it was the most current version at the time of the study. All parameters used in this study are introduced here, followed by a detailed description of the methods common to all specific aims and, finally, an explanation of details unique to each specific aim.

2.1 Description of Parameters

2.1.1 Commissioning Parameters

A list of parameters relevant to SmartArc planning was created and categorized into two groups: commissioning parameters and planning parameters. Commissioning parameters were those parameters available for selection during the commissioning and configuration of the linear accelerator in the treatment planning system. These parameters included dose rate, gantry speed, MLC size and maximum leaf speed, and maximum MU per degree of rotation. These parameters are typically chosen based on the physical and mechanical capabilities of the linear accelerator used for treatment, and are briefly described here:

- Dose rate is a measure of the output of the beam in MU per time. The Philips Pinnacle treatment planning system allows for the dose rate to be varied either continuously or discretely. The user must also specify a maximum allowable dose rate. If the dose rate is varied continuously, the user must only provide the maximum allowable dose rate as input to Pinnacle. If the dose rate is varied discretely, the user must provide each allowable dose rate in a table provided in the commissioning window of Pinnacle. Elekta linear accelerators vary dose rate discretely, stepping down from the maximum dose rate

by a factor of two until reaching some minimum dose rate (i.e. 600, 300, 150, 75, 37 MU/min). Varian linear accelerators, however, have a continuously variable dose rate. In this study, trials for both continuously variable and discretely variable dose rates were examined for maximum dose rates of 400, 600 and 800 MU/min.

- Maximum gantry speed describes the maximum angular velocity of the gantry, and is given in units of degrees per second. The maximum gantry speed would theoretically influence resulting VMAT plans because the gantry is continuously rotating as the beam is continuously delivering. A faster maximum speed implies the possibility of a shorter overall delivery and perhaps a better dose distribution. The faster gantry lowers the minimum possible dose delivered per control point arc. Maximum gantry speeds of 4, 6, 8, and 12 deg/sec were used in this study.
- Maximum MLC leaf speed is a measure of how far the leaves can travel in a certain amount of time in units of cm/sec. The relevance of this parameter is connected to gantry rotation speed. The distance the leaves can travel per gantry rotation determines how much the beam shape can change between control points, and how much the beam can be modulated by the MLC. Only IMRT delivery techniques using dynamic MLC would be influenced by this parameter. Maximum MLC leaf speeds used in the study were 1, 2, and 3 cm/sec.
- MLC leaf size describes the width of the individual MLC leaves and varies among linear accelerator vendors. Leaves in the 80-leaf MLC of Elekta linear accelerators have 1cm thickness, while the 120-leaf Varian MLC combines 5mm leaves in the center of the field with 1cm leaves toward the edges of the field. It would be intuitive to assume a smaller MLC leaf size would produce a more conformal dose to the PTV and spare normal

tissues surrounding the PTV more effectively. In fact, it has been shown that this is not necessarily the case for fixed-beam IMRT (Su *et al.* 2007). Leaf widths of 1cm and 5mm were both used in this study.

- Maximum MU/degree limits how much output the beam can deliver per degree of rotation. The starting value for this study was 100 MU/deg, and then 1 MU/deg was chosen to determine how the optimization algorithm would respond to an unreasonably low value.

Commissioning parameters do not necessarily have an effect on optimization of fixed-beam IMRT treatments. For example, the leaf speed and gantry rotation do not affect the plan quality of a step-and-shoot treatment because the leaves are not moving and the gantry is not rotating while the dose is being delivered. However, commissioning parameters could have an important influence on plan quality for VMAT treatments because the gantry rotates and the MLC moves continuously during beam delivery. A list of commissioning parameters and the range of values for which each parameter was varied is given in Table 2-1. The intervals of values chosen for parameter variation were selected to bind the possible capabilities of a linear accelerator around a

Table 2-1. List of commissioning parameters and range of values used in the study. Baseline values shown in bold type.

Commissioning Parameters	Range of values
Gantry Speed Variability	**yes**/no
Maximum Gantry Speed	4, **6**, 8, 12 deg/sec
Maximum Dose Rate	400, **600**, 800 MU/min
Dose Rate Variability	Continuous/**Discrete**
Maximum MLC Leaf Speed	1, **2**, 3 cm/sec
MLC Leaf Size	**1cm**/5mm
Maximum MU/degree	1, **100** MU/deg

baseline value, shown in bold type in Table 2-1. Baseline values were chosen according to recommendations from Pinnacle (Friberger 2009) and existing machine capabilities.

2.1.2 Planning Parameters

Planning parameters were defined as those parameters available for selection during routine treatment planning. Planning parameters examined in this work included beam energy, arc length, collimator angle, dose grid resolution, final gantry spacing, and maximum delivery time, and are briefly described here:

- Beam energy depends on a selection of megavoltage energies available for any specific machine. The machine used in the present study had 6, 10, and 15 MV energies available.
- Arc length is determined by setting the start and stop angle of the continuous arc. Pinnacle version 8.1y used in this study could only optimize for a single, maximum 360-degree arc. For this study, total arc lengths were varied to 60, 120, 180, 270, and 360 degrees.
- Collimator angle ranges from 0 to 360 degrees and remains stationary throughout the entire treatment. MLC leaves move in only one dimension, so the collimator can move parallel to gantry rotation direction (90 degree collimator angle for this study) or perpendicular to gantry rotation direction (0 degree collimator angle for this study) or at some angle in between. A 45 degree collimator angle covers the longest distance in the superior-inferior dimension. Collimator angles of 0-90 degrees represent a complete range of collimator orientations with respect to gantry rotation direction. For instance, collimator angles of 0 and 180 degrees represent the same orientation to gantry rotation, and collimator angles of 90 and 270 degrees represent the same orientation to gantry

rotation. For this reason, only collimator angles ranging from 0 to 90 degrees were used in this study.

- Dose grid resolution determines the dose calculation sampling resolution for the Pinnacle treatment planning system. The standard dose grid resolution used in our treatment facility is 0.400 cm. Dose grid resolution was also varied to 0.300cm and 0.500 cm to determine the effects on resulting plan quality.
- Final gantry spacing is the final spacing of control points around the VMAT delivery arc. Because of progressive sampling, described earlier, the optimization always starts at a 24 degree spacing of control points, and the final spacing is chosen by the user to be 2, 3, 4, or 6 degrees.
- Maximum delivery time is requested by the user to keep overall treatment time less than some maximum value. Maximum delivery times used in this study were 60, 120, and 240 seconds for all treatment geometries, with varying supplemental treatment times for each geometry.
- Allow backup jaw motion parameter determines if the jaws remain stationary or if they are allowed to follow the MLC leaves during treatment. Allowing back-up jaw motion during optimization created an artifact in the computed final dose in version 8.1y, so jaws were opened enough to cover the PTV with a 0.5cm margin from all gantry angles at specified collimator setting and fixed in position for optimization for this study. In more recent versions of Pinnacle (9.0), this problem has been resolved.

Planning parameters are not necessarily limited by linear accelerator capabilities, but are an integral part of the optimization process for SmartArc treatment planning. They are typically

variable within the machine's capabilities and chosen by the planner to create the best possible plan.

In addition to planning parameters used for several different delivery techniques, there are a few planning parameters specific to SmartArc optimization. One of these parameters, final gantry spacing, determines the final spacing of control points around the delivery arc. Maximum delivery time is also unique to SmartArc optimization and allows the user to minimize overall treatment time per treatment fraction. A complete list of planning parameters used in this study and the interval of values for which they were varied is given in Table 2-2. Baseline values are shown in bold type. These values were chosen according to recommendations by Pinnacle and common values used for fixed-beam IMRT in our treatment facility.

Table 2-2. List of planning parameters and range of values used in this study. Baseline values are shown in bold type.

Planning Parameters	Range of values
Beam Energy	**6**, 10, 15 MV
Arc Length	60, 120, 180, 270, **360** deg
Collimator angle	**0**, 30, 45, 60, **90** deg
Dose grid resolution	0.3, **0.4**, 0.5 cm
Maximum delivery time	60, **120**, 240 sec
Final gantry spacing	2, 3, **4**, 6 deg

2.2 Research Design

This study focused on three treatment sites to determine the effect of varying each of the previously mentioned parameters on plan quality: a spherical target within a cylindrical phantom, a single-target prostate, and a multi-target prostate. Each of the three specific aims tested the hypothesis for one and only one of these treatment sites. The process for creating treatment plans and evaluating commissioning and planning parameters was common to all aims and is described in the following paragraphs. First, a clinically acceptable baseline plan was generated for each treatment geometry. Then, parameters were varied independently and systematically

from their baseline values. Finally target homogeneity data, conformity data, and normal tissue data were collected in order to quantify and evaluate the quality of resulting plans.

2.2.1 Baseline Plan

For each treatment site, a baseline plan was created that provided acceptable dose homogeneity and sufficient normal tissue sparing. To determine sufficient normal tissue sparing and clinical acceptability, all baseline plans were approved by a radiation oncologist. Initial parameter values for each baseline plan were set based on recommendations from Pinnacle or taken as values from an Elekta linear accelerator used for IMRT treatment at our facility. Baseline parameter values are shown in Table 2-3.

Table 2-3. Baseline parameter values for all three treatment geometries.

Parameter	Baseline Value
Gantry Speed Variability	yes
Maximum Gantry Speed	6 deg/sec
Maximum Dose Rate	600 MU/min
Dose Rate Variability	Discrete
Maximum MLC Leaf Speed	2 cm/sec
MLC Leaf Size	1cm
Maximum MU/degree	100 MU/deg
Beam Energy	6 MV
Arc Length	360 deg
Collimator angle	0 (prostate), 90 (phantom) deg
Dose grid resolution	0.4 cm
Maximum delivery time	120 sec
Final gantry spacing	4 deg

2.2.2 Parameter Variation

Once a baseline plan was created, all commissioning and planning parameters were varied systematically. Figure 2-1 shows a diagram of how each parameter was varied. After the treatment geometry was selected and the baseline parameter values were chosen, the baseline

plan was copied several times, creating a new plan for each parameter in order to study parameters separately.

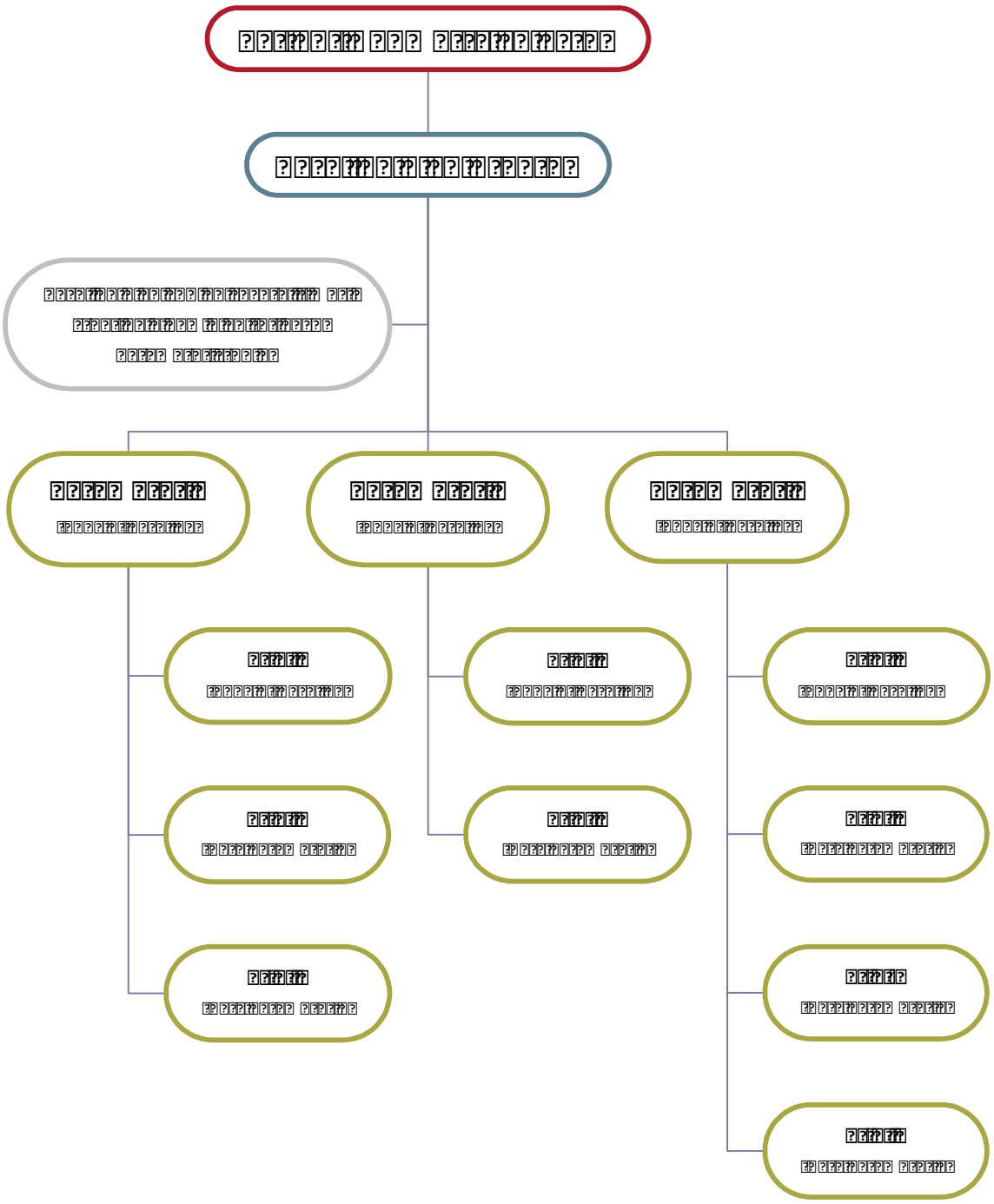

Figure 2-1. Diagram of steps taken to create new trials for each parameter studied. First patient geometry is selected, then a baseline plan is created and copied several times to create a new plan for each parameter studied. The baseline trial is then copied within each plan in order vary that parameter while keeping all other parameters set to their baseline values.

Several trials were created within each plan corresponding to different input values for that parameter. For example, a plan entitled "Maximum gantry speed" was created for each patient, and several trials were created inside that plan with different maximum gantry speeds. To examine commissioning parameters, it was necessary to commission a new machine for each trial.

Copying the baseline plan generated a baseline trial within every plan. Each parameter was varied from a copy of this baseline trial. In other words, the baseline plan was copied several times to create new plans (one plan for every commissioning and planning parameter), and the baseline trial was copied several times to create new trials within those plans. This assured that all parameters remained fixed at the baseline values except for the parameter being studied in that plan. The number of trials in each plan depended on the range of variability of the parameter being studied. Some parameters consisted of a yes or no option; therefore these plans contained only two trials. The range of variability was chosen to expand above and below the baseline value for each parameter, and is shown for commissioning and planning parameters in Tables 2-1 and 2-2. Table 2-1 shows 6 commissioning parameters with 16 unique settings, and Table 2-2 shows 6 planning parameters with 23 unique settings. For this study, parameters were varied independently to determine their individual effect on resulting plan quality, as varying all combinations of parameters (almost 800,000 possibilities) together would be impractical using a systematic approach.

2.2.3 Plan Evaluation

Plans from each trial were compared and evaluated using the dose volume histograms (DVHs) calculated by Pinnacle, the dose homogeneity index (DHI) for each PTV, the conformity

index (CI) for the primary PTVs of each treatment geometry, and the dose to normal tissue metrics. The DHI was calculated as

$$DHI = \frac{D_{\max(1\%)} - D_{\min(99\%)}}{D_{prescribed}}, \quad (1)$$

where $D_{min(99\%)}$ is the dose exceeded by 99% of the target volume and $D_{max(1\%)}$ is the dose exceeded by 1% of the target volume. This was done in order to avoid including artificially high and low dose regions created by Pinnacle's dose computation and/or small volumes of little clinical interest. A perfectly homogenous dose to the PTV would result in a DHI of 0.0. The conformity index (CI) was also used to evaluate the quality of each plan. The conformity index measures how well the prescription dose conforms to the target volume, and it is defined as

$$CI = \left(\frac{TV_{PIV}}{TV}\right) \times \left(\frac{TV_{PIV}}{PIV}\right), \quad (2)$$

where PIV is the volume covered by the prescribed isodose value, TV is the volume of the target, and TV_{PIV} is the volume of the target within the prescribed isodose value. Ideally the PIV, TV, and TV_{PIV} would be equal, making the CI equal to 1.

For the two cases involving normal tissue constraints (simple prostate and complex prostate), normal tissue metrics were also used to evaluate the plan quality. "Hard" constraints for normal tissues for intact prostate cancer treatment are described by Pollack *et al*. (2005): ≤17% and ≤35% of the rectal volume receives ≥65Gy and ≥40Gy, respectively; ≤25% and ≤50% of the bladder volume receives ≥65Gy and ≥40Gy, respectively; and ≤10% of each femoral head receives ≥50Gy. One of the absolute conditions for clinical acceptability of these prostate plans was that 95% or greater of the PTV received 100% of the prescribed dose. For this reason, all

prostate plans in our study were normalized so that 95% of the PTV received the prescription dose. Normal tissue metrics were taken from Pollack *et al.*, and evaluated at 17% and 35% of the rectum, 25% and 50% of the bladder, and 10% of the femoral heads. The maximum dose to the femoral heads were also evaluated, taken at $D_{max(1\%)}$. The phantom case had no normal tissue constraints, so only the DHI and CI were used in evaluating parameter trials for the phantom case.

2.3 Specific Aims

Three treatment geometries of increasing complexity were chosen for this study in order to determine the effect of varying both *commissioning* and *planning* parameters on resulting plan quality. Each specific aim examined a single treatment geometry. The following sections describe the details unique to each specific aim.

2.3.1 Specific Aim 1: Phantom Case

The first geometry, a phantom, was chosen to represent an ideal case for treatment. Because it was important to start with the simplest conceivable case to determine an upper threshold for the capabilities of SmartArc optimization, the phantom geometry can be described as a simple approximation of a prostate PTV without any dose limiting structures. For the phantom geometry, a spherical target was contoured in the center of a cylindrical, homogeneous, water-equivalent phantom. The target was 7.5 inches in diameter, and it was centered inside the 30-inch diameter cylinder. A cylindrical phantom was chosen instead of a rectangular phantom because it was believed to better represent the contour of the human body. The spherical target was drawn using Pinnacle software in the center of the phantom, and there were no avoidance structures identified. The prescription given to the phantom target for optimization was 200 cGy to 95% of the PTV in 1 fraction, which represents a typical fractional dose for prostate cancer at

our treatment facility. Because the tabular DVHs calculated by Pinnacle show dose in cGy, the phantom plans were later prescribed 7600 cGy in 38 fractions to achieve a better dose resolution for gathering data from the DVHs. Changing the number of fractions in the prescription did not change the fractional DVH; all data points were merely multiplied by a factor of 38. A transverse view of the phantom geometry is shown in Figure 2-2.

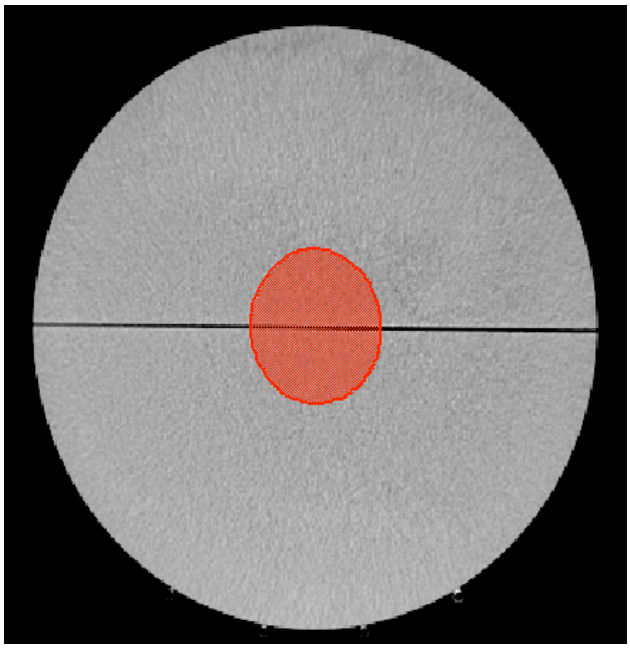

Figure 2-2. Transverse view of phantom case. PTV is shown in red.

2.3.2 Specific Aim 2: Simple Prostate Case

The second geometry was a single-target prostate patient. This case was chosen because it represented a relatively standard, simple prostate case. The patient selected had previously been treated at our facility with fixed-beam, 7-field step-and-shoot IMRT. The original prescription was 7600 cGy to the PTV in 38 fractions delivered with a 6MV beam, and avoidance structures included the rectum, bladder, and left and right femoral heads. The prescription for this study was kept the same as the original prescription. Transverse, sagittal, and coronal views of the simple prostate geometry are shown in Figure 2-3.

Figure 2-3. Transverse (top), sagittal (left), and coronal (right) view of simple prostate case. PTV is shown in red.

2.3.3 Specific Aim 3: Complex Prostate Case

The third geometry used in this study was a complex prostate case with multiple PTVs. This treatment site was chosen to represent a more complicated geometry. The patient was previously treated at our facility with helical tomotherapy. The original prescription was 56 Gy in 28 fractions to the extended prostate bed with a 22 Gy boost to the prostate bed; 61.6 Gy in 28 fractions to a positive node; and 46.2 Gy in 28 fractions to the entire nodal region. Avoidance structures included the rectum, bladder, and left and right femoral heads. The prescription for the SmartArc optimization was 78 Gy to the prostate bed (PTV 1), 61.6 Gy to the positive node (PTV 2), 56 Gy to the extended prostate region (PTV 3), and 46.2 Gy to the extended nodal region (PTV 4) in 28 fractions. Transverse, sagittal, and coronal views of the complex prostate treatment geometry are shown in Figure 2-4.

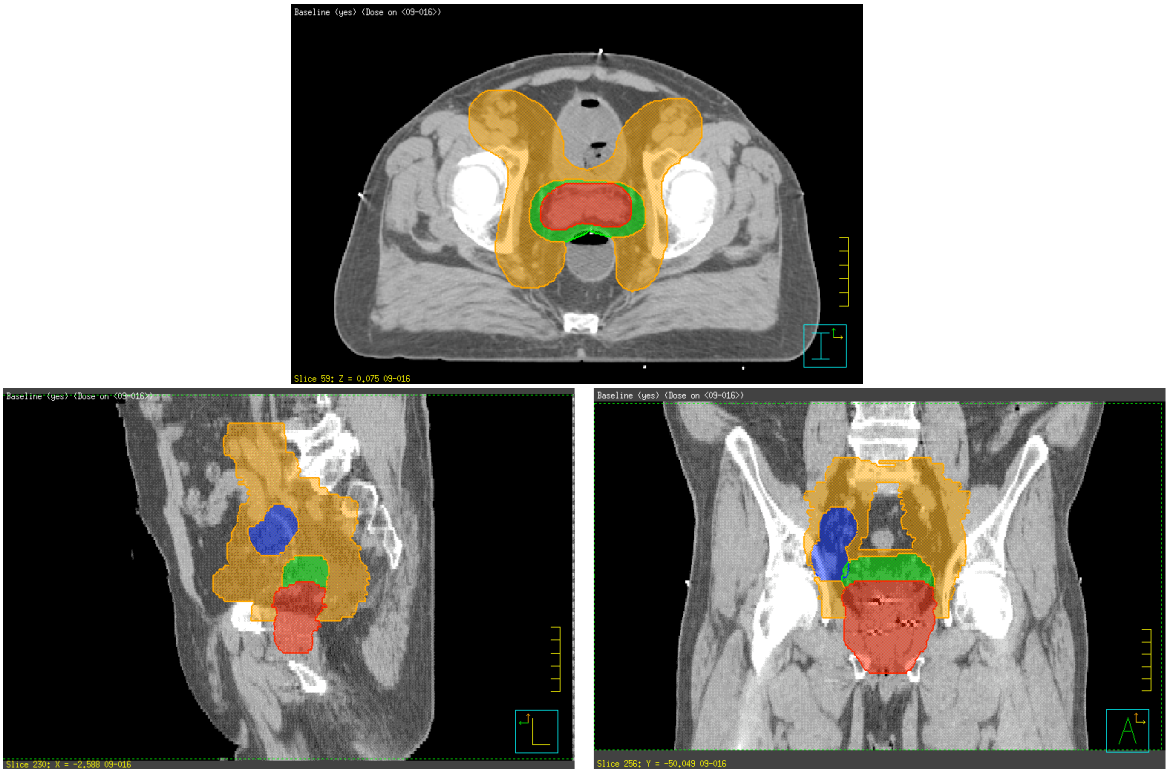

Figure 2-4. Transverse (top), sagittal (left), and coronal (right) views of complex prostate geometry. PTV1: red, PTV2: green, PTV3: blue, PTV4: orange.

3 RESULTS

This chapter describes the resulting plans based on metrics taken from the dose volume histograms (DVHs), dose homogeneity indices (DHI), conformity indices (CI), and normal tissue metrics. The results for the three baseline plans are described first, and then data for each commissioning and planning parameter is presented simultaneously for all three specific aims.

3.1 Baseline Results

3.1.1 Phantom Baseline Results

A baseline plan was created to achieve acceptable dose homogeneity to the target for the phantom case. A transverse image of the baseline plan is shown in Figure 3-1, where the red shaded area represents the PTV. The corresponding DVH for the phantom baseline plan is shown in Figure 3-2. A single, 360-degree dynamic arc beam with energy 6MV was used for the baseline plan, and the isocenter for this beam was placed in the center of the target volume. The plan was allowed 35 iterations, but a solution was found in only 21 iterations. The convolution dose calculation started at iteration 8. The only optimization objectives set for this aim, listed in Table 3-1, were maximum and minimum dose to the PTV. The prescription isodose line (7600cGy) is shown in Figure 3-1, along with the prescription ±3% isodose lines (7372cGy and 7828cGy). All baseline commissioning and planning parameter values were discussed previously and are shown in Table 2-3. All trials were normalized so that at least 95% of the PTV received 100% of the prescribed dose. The optimization took approximately 15 minutes for each trial (excluding smaller arc lengths) for the phantom case, and final dose computation took about 20 minutes to complete for each trial.

Table 3-1. Optimization objectives for phantom case, Aim 1

ROI	Type	Target cGy	Weight
PTV	Max Dose	205	10
PTV	Min Dose	195	10

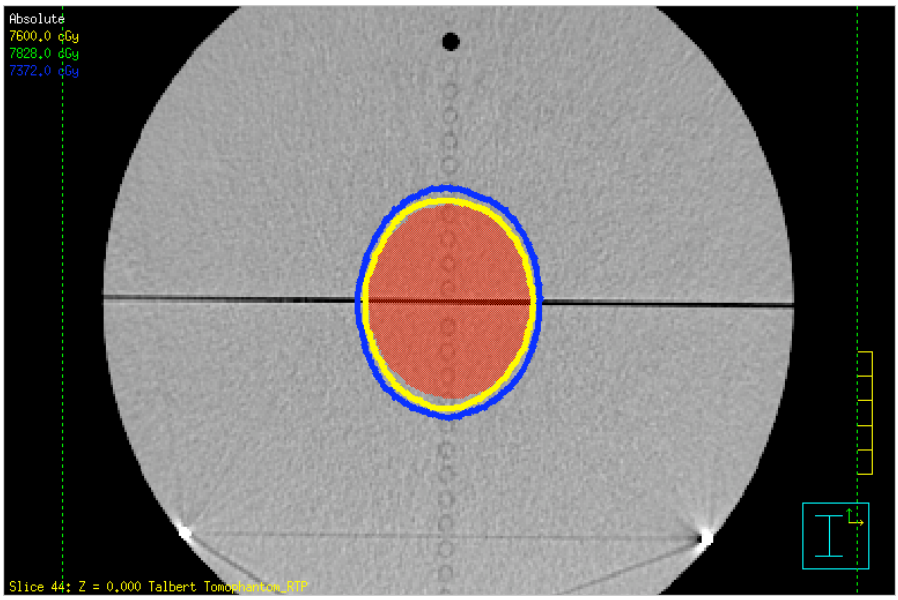

Figure 3-1. Phantom baseline plan isodose lines (blue: 97%, yellow: 100%, green: 103% of prescribed dose)

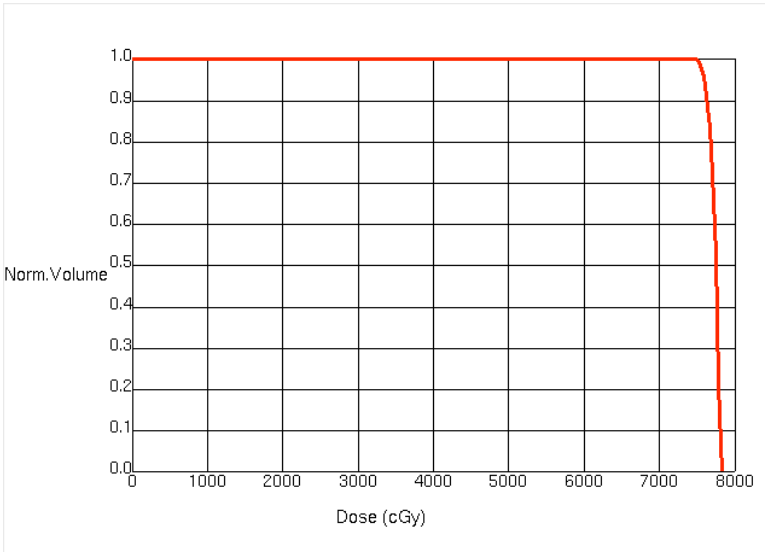

Figure 3-2. DVH for the phantom baseline plan. PTV: red, no avoidance structures.

3.1.2 Simple Prostate Baseline Results

A baseline plan was created to achieve ±5% dose homogeneity to the simple prostate target. A single, 360-degree dynamic arc beam with an energy of 6MV was used for the baseline plan, and the isocenter for this beam was placed in the center of the prostate PTV. The optimization was allowed 45 iterations, with the convolution dose calculation starting at iteration

8. Figure 3-3 shows a transverse slice of the baseline plan for the simple prostate patient including isodose lines for the prescription dose (7600cGy) and ± 5% of the prescription dose (7372cGy and 7828cGy). Optimization objectives for the simple prostate case were kept very similar to the optimization objectives of the original plan with only minor tuning in order to reach homogeneity goals. A complete list of optimization objectives for the simple prostate case

Table 3-2. Optimization objectives for simple prostate case, Aim 2

ROI	Type	Target cGy	% Volume	Weight
PTV 76	Max dose	7800	-	10
PTV 76	Min dose	7300	-	10
PTV 76	Min DVH	7600	95	45
76 only	Max dose	7600	-	1
Ring	Max dose	3800	-	1
Rectum	Max DVH	3500	45	1
Rectum	Max DVH	7000	8	1
Rectum	Max DVH	6500	15	1
Bladder	Max DVH	4000	45	1
Bladder	Max DVH	6000	20	1
LFH	Max dose	4300	-	1
RFH	Max dose	4300	-	1

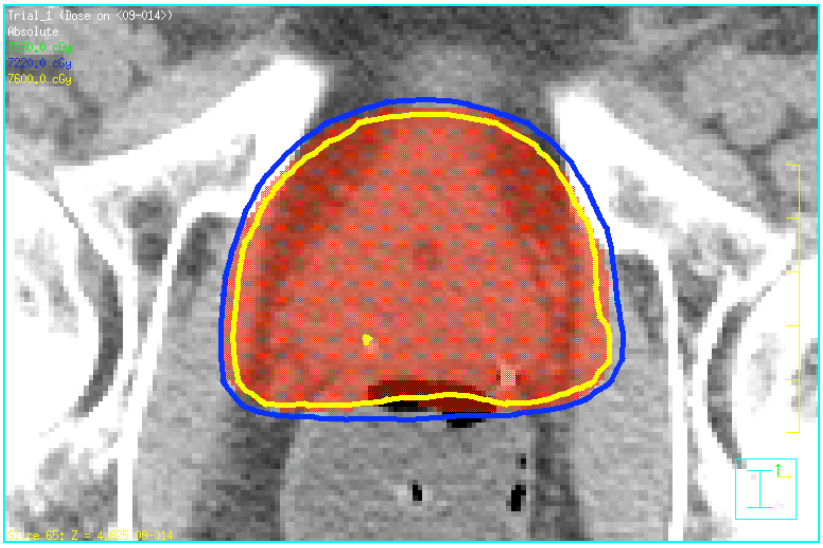

Figure 3-3. Simple prostate baseline plan isodose lines (blue: 95%, yellow: 100%, green: 105% of prescribed dose)

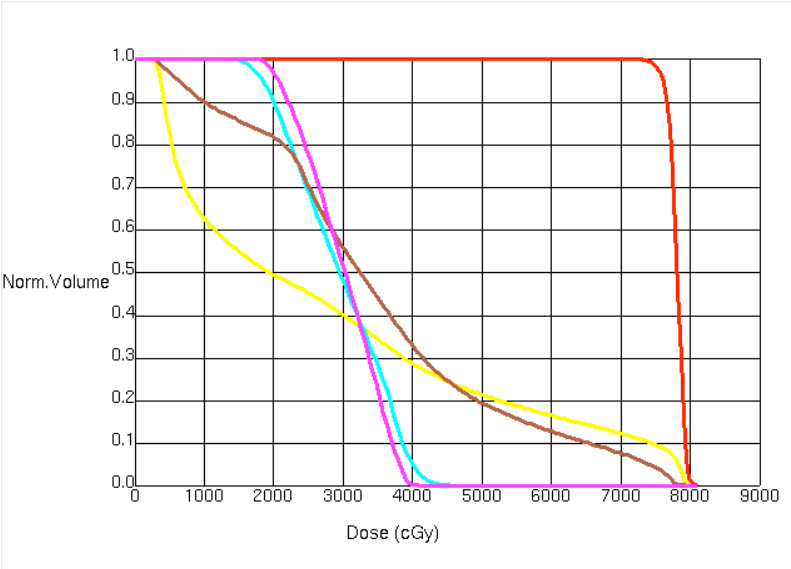

Figure 3-4. DVH for the simple prostate baseline plan. PTV: red, rectum: brown, bladder: yellow, right femoral head: purple, left femoral head: blue.

is given in Table 3-2. All baseline commissioning and planning parameter values for the simple prostate case were discussed previously and are shown in Table 2-3. After the baseline plan was created, the DVH for the plan, shown if Figure 3-4, was approved by a radiation oncologist. It was determined that the baseline plan was clinically acceptable for treatment based on dose homogeneity to the target volume and normal tissue constraints. All trials were normalized so that at least 95% of the PTV received 100% of the prescribed dose. The optimization took approximately 40 minutes for each simple prostate trial (excluding smaller arc lengths), and final dose computation took roughly 50 minutes to complete for each trial.

3.1.3 Complex Prostate Baseline Results

A baseline plan was created for the complex prostate case, attempting to achieve ±5% dose homogeneity to the primary PTV. This homogeneity goal was not achieved, and the better of two possible baseline plans was chosen by a radiation oncologist. Figure 3-5A and 3-5B show transverse and saggital views of the patient where all 4 PTVs are visible. The prostate bed

Table 3-3. Optimization objectives for complex prostate case, Aim 3

ROI	Type	Target cGy	% Volume	Weight
PTV 78	Max Dose	7900	-	100
PTV 78	Min Dose	7600	-	100
PTV 78	Uniform Dose	7800	-	100
7800 ring	Max Dose	7800	-	1
PTV 6160	Uniform Dose	6160	-	75
6160 ring	Max Dose	6160	-	1
PTV 56	Min DVH	5600	95	1
5600 only	Uniform Dose	5600	-	1
PTV 4620	Min DVH	4620	95	30
4620 only	Uniform Dose	4620	-	25
Ring 1	Max Dose	3500	-	1
Rectum	Max DVH	6500	17	20
Rectum	Max DVH	4000	35	30
Bladder	Max DVH	6500	25	20
Bladder	Max DVH	4000	50	20
LFH	Max Dose	4200	-	40
RFH	Max Dose	4200	-	40

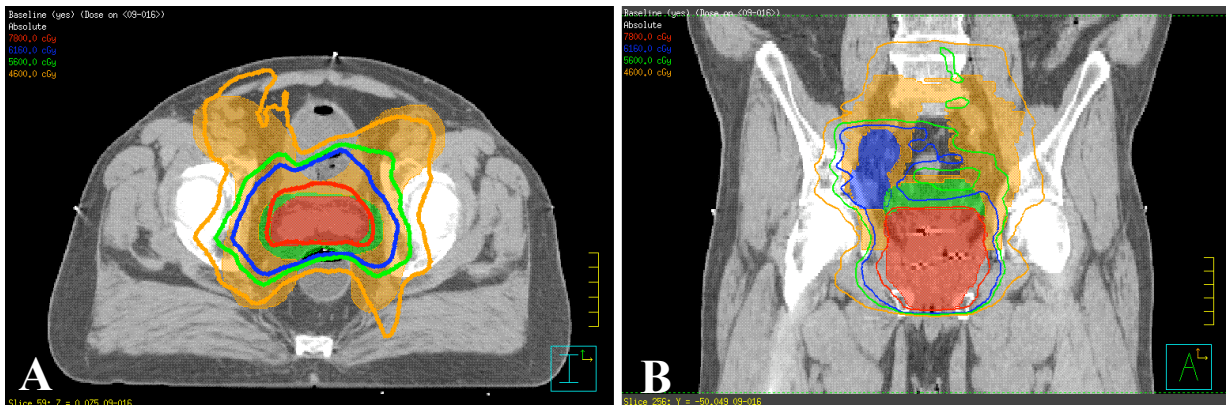

Figure 3-5. Complex prostate baseline plan transverse (A) and sagittal (B) views. Shaded areas represent PTVs, and corresponding lines represent 100% of the prescribed dose for each PTV. PTV1 (7800cGy): red, PTV2 (6160cGy): blue, PTV3 (5600cGy): green, PTV4 (4620cGy): orange.

is shown in red (PTV 1; 7800 cGy), the extended prostate shown in dark blue (PTV 3; 5600 cGy), the positive node in purple (PTV 2; 6160 cGy), and the extended nodal region in light blue (PTV 4; 4620 cGy). Figure 3-6 shows the DVHs for all PTVs and critical structures for the complex prostate case. A single, 360-degree dynamic arc beam with energy 6MV was used for

the baseline plan, and the isocenter was placed in the center of the composite target volumes. The plan was allowed 35 iterations, with the convolution dose starting at iteration 10. Optimization objectives for the complex prostate case baseline plan are shown in Table 3-3. Because the patient was previously treated with helical tomotherapy, there was no previous set of optimization objectives for the Pinnacle treatment planning system. Optimization objectives and additional regions of interest (such as rings) were created to achieve a clinically acceptable baseline plan. The baseline plan for the multi-target prostate case was determined to be clinically acceptable by a radiation oncologist, though the "hard" normal tissue constraints described by Pollack *et al.*, for the most part, were not met. The baseline set of parameters was identical to the single-target prostate case. Baseline commissioning and planning parameters are shown in Table 2-3.

All trials were normalized so that at least 95% of the PTV received 100% of the prescribed dose. The optimization took approximately 45 minutes for each complex prostate

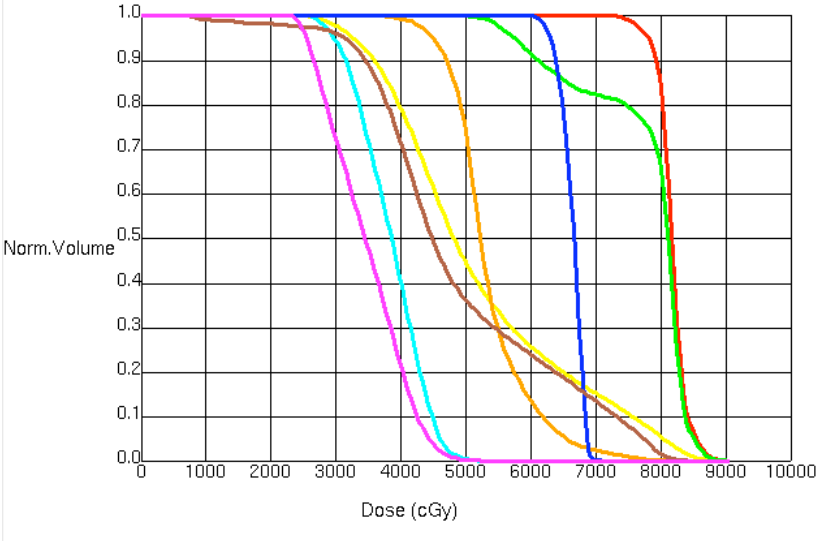

Figure 3-6. DVH for the complex prostate baseline plan. PTV1: red, PTV2: dark blue, PTV3: green, PTV4: orange, rectum: brown, bladder: yellow, right femoral head: purple, left femoral head: light blue.

trial (excluding smaller arc lengths), and final dose computation took roughly 80 minutes to complete for each trial.

3.1.4 Baseline DHI and CI Values

Values of DHI, CI, and normal tissue metrics for the baseline plans are shown in Tables 3-1 to 3-3. DHI was lowest for the phantom case and highest for the PTVs of the complex prostate case. CI was highest for the simple prostate case and lowest for the complex prostate case. It is believed that CI performed better for the simple prostate case than the phantom case because the phantom case had no avoidance structures. Normal tissue sparing was better for the simple prostate case than the complex prostate case.

Table 3-4. Baseline values for DHI, D_{max}, and D_{min} for PTVs of the three treatment geometries, shown in cGy.

Geometry (Dose Rx to 95% PTV)	PTV $D_{min(99\%)}$	PTV $D_{max(1\%)}$	DHI
Phantom (76 Gy)	7540	7812	0.0358
Simple Prostate (76 Gy)	7447	8006	0.0736
PTV 1 (78 Gy)	7481	8744	0.1619
PTV 2 (61.6 Gy)	6133	6918	0.1274
PTV 3 (56 Gy)	5333	8721	0.6050
PTV 4 (46.2 Gy)	4047	7456	0.7379

Table 3-5. Baseline values for CI for the three treatment geometries.

Geometry	CI
Phantom	0.8777
Simple Prostate	0.9106
Complex Prostate (PTV1)	0.7900

Table 3-6. Baseline values for normal tissue metrics for prostate geometries, shown in cGy.

Geometry	Rectum		Bladder		Rt. Fem. Head		Lt. Fem. Head	
	D_{17}	D_{35}	D_{25}	D_{50}	D_{10}	$D_{max(1\%)}$	D_{10}	$D_{max(1\%)}$
Simple Prostate	5297	3893	4420	1927	3702	3927	3855	4248
Complex Prostate	6666	5066	6054	4811	4250	4748	4477	4868
Pollack et al. (2008) limit	6500	4000	6500	4000	5000	--	5000	--

3.2 Commissioning Parameters

3.2.1 Gantry Speed Variability

DHI, CI, and normal tissue values for gantry speed variability are shown in Tables 3-4 and 3-5. The DHI showed no change for the phantom and complex prostate cases and varied less than 2% for the simple prostate case. In fact, the phantom and complex prostate cases showed identical plans for both trials, and the simple prostate case showed little difference in the resulting plans.

The CI showed no change for the phantom and complex prostate cases and differed by less than 0.03 between trials for the simple prostate case.

Table 3-7. DHI and CI values for Gantry Speed Variability (PTV 1: 78Gy, PTV 2: 61.6Gy, PTV 3: 56Gy, PTV 4: 46.2Gy).

Dose Homogeneity Index

Gantry Speed	Phantom	Simple Prostate	Complex Prostate			
			PTV 1	PTV 2	PTV 3	PTV 4
Variable (max 6 deg/sec)	**0.0358**	**0.0736**	**0.1619**	**0.1274**	**0.6050**	**0.7379**
not variable (6 deg/sec)	0.0358	0.0866	0.1619	0.1274	0.6050	0.7379

Conformity Index

Gantry Speed	Phantom	Simple Prostate	Complex Prostate
Variable (max 6 deg/sec)	**0.8777**	**0.9106**	**0.7900**
not variable (6 deg/sec)	0.8777	0.8956	0.7900

Table 3-8. Normal tissue metrics for Gantry Speed variation for simple and complex prostate cases. All normal tissue dose metrics are shown in cGy.

Gantry Speed	Norm. %	Rectum		Bladder		Rt. Femoral Head		Lt. Femoral Head	
		D_{17}	D_{35}	D_{25}	D_{50}	D_{10}	$D_{max(1\%)}$	D_{10}	$D_{max(1\%)}$
Simple Prostate									
variable	**95.4**	**5297**	**3893**	**4420**	**1927**	**3702**	**3927**	**3855**	**4248**
not variable	95.4	5371	3955	4458	1906	3767	4023	3820	4209
Complex Prostate									
variable	**95**	**6666**	**5066**	**6054**	**4811**	**4250**	**4748**	**4477**	**4868**
not variable	95	6666	5066	6054	4811	4250	4748	4477	4868

Absolute dose values for normal tissue metrics for the two prostate cases are shown in Table 3-5. Normal tissue metrics were within 3% of the baseline values for the simple prostate case, and did not change for the complex prostate case. Resulting plans showed no significant dependence on allowing the gantry speed to vary during treatment.

3.2.2 Maximum Gantry Speed

The maximum gantry speed was varied above and below that of the baseline plan (6 deg/sec) to determine if a faster or slower rotation speed would improve or degrade the plan quality. The resulting DHI and CI are graphed in Figures 3-7 to 3-9.

Figure 3-7 shows that DHI values for the phantom were the lowest, and DHI values for the complex prostate PTV 1 were highest. This was the case for all parameters studied. The DHI for the phantom and simple prostate cases varied by less than 0.02 as the maximum gantry speed increased from 4 deg/sec to 12 deg/sec. The variation in DHI for the baseline trial and DHI for 12 deg/sec trial for PTV1 was 0.026, and the 12 deg/sec trial performed best.

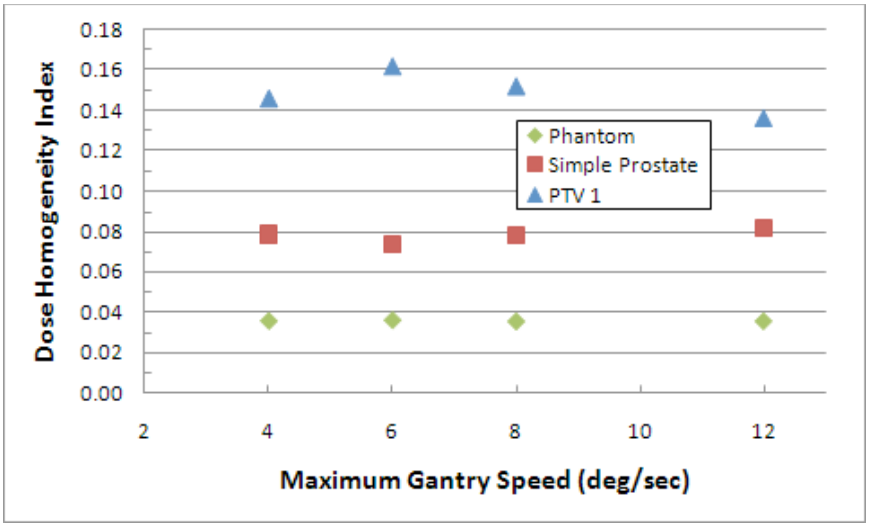

Figure 3-7. DHI for "Maximum Gantry Speed" parameter: phantom (green), simple prostate (red), and PTV 1 (blue) of complex prostate case.

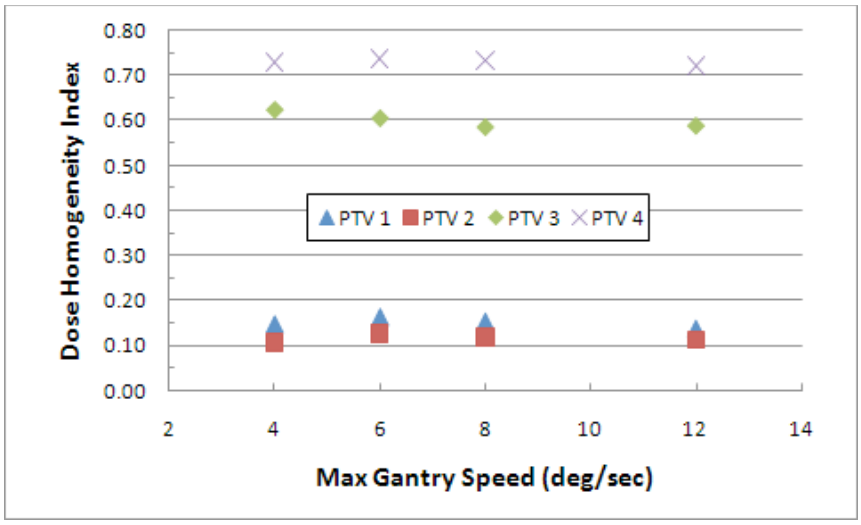

Figure 3-8. DHI for "Maximum Gantry Speed" parameter: PTV 1 (blue), PTV 2 (red), PTV 3 (green), and PTV 4 (purple) of complex prostate case.

The data in Figure 3-8 shows that the DHI values for PTV 3 and PTV 4 were much greater than the DHI values for PTV 1 and PTV 2. This indicates that the dose to PTV 3 and PTV 4 was less homogeneous than the dose to PTV 1 and PTV 2.

Resulting CI values are plotted for varying maximum gantry speed in Figure 3-9. The variation in CI values across all maximum gantry speeds for the phantom and simple prostate

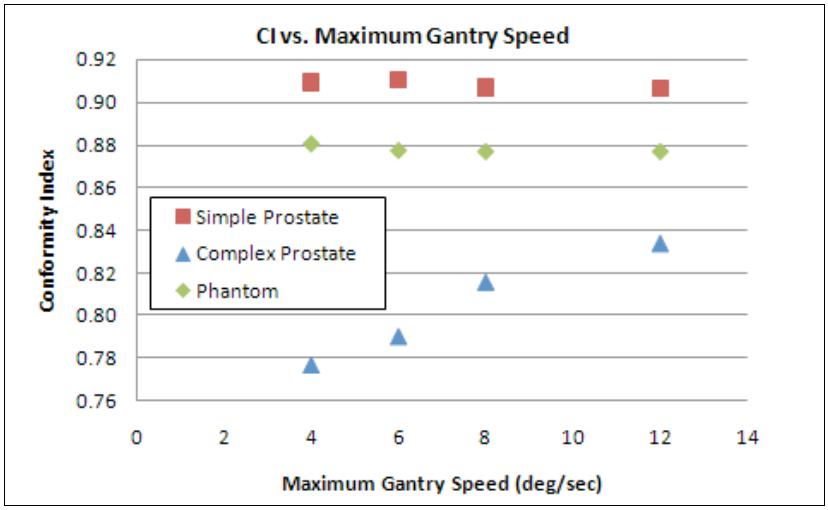

Figure 3-9.CI for "Maximum Gantry Speed" parameter: phantom (green), simple prostate (red), and complex prostate (blue) cases.

cases was less than 0.02. The variation in CI values between the baseline trial and 12 deg/sec trial for the complex prostate case was 0.044, improving as the maximum gantry speed increased.

Normal tissue metrics for variation of maximum gantry speed are plotted in Figure 3-10 for the two prostate cases. The normalized dose is plotted against the maximum gantry speed for all normal tissue metrics. The two dotted lines represent 2% above and below the baseline dose

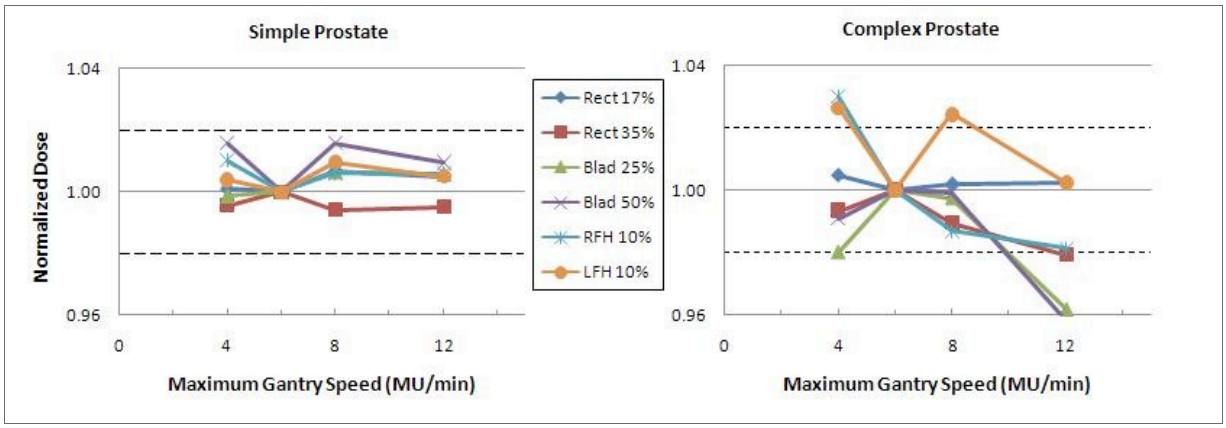

Figure 3-10. Normal tissue metrics for "Maximum Gantry Speed" parameter for simple prostate and complex prostate cases. All doses normalized to dose values for the baseline trial (6deg/sec).

value. Dose values for all metrics were normalized to those of the baseline plan; therefore, all plots intersect at 6 deg/sec, the baseline setting for this parameter. It is evident from the simple prostate graph that all variations for normal tissue dose metrics were within 2% of the baseline dose value. The complex prostate normal tissue metrics varied more than 2% for some normal tissue metrics, but generally improved (lower dose) as the maximum allowable gantry speed increased.

3.2.3 Maximum Dose Rate

Figures 3-11 and 3-12 show DHI values plotted for the phantom case, simple prostate case, and complex prostate case. Both continuously variable dose rates (circles) and discretely

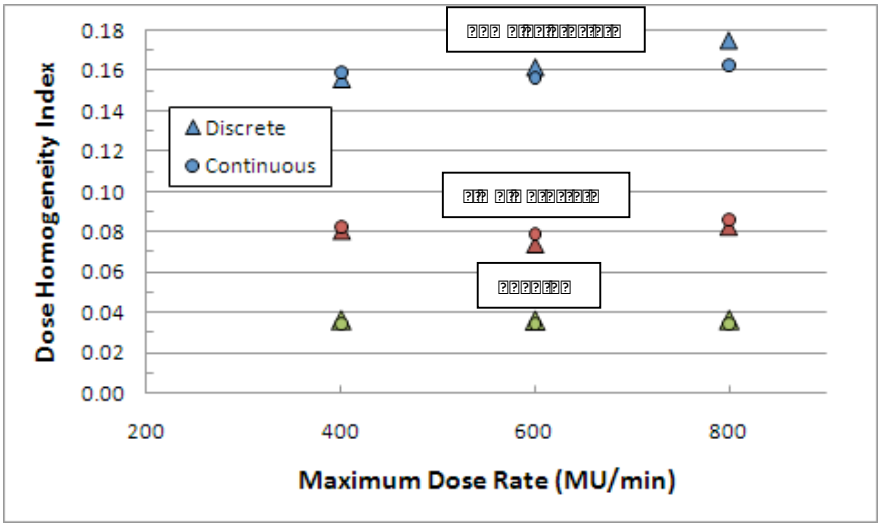

Figure 3-11. DHI for "Maximum Dose Rate" parameter: phantom (green), simple prostate (red), and PTV 1 (blue) of complex prostate case.

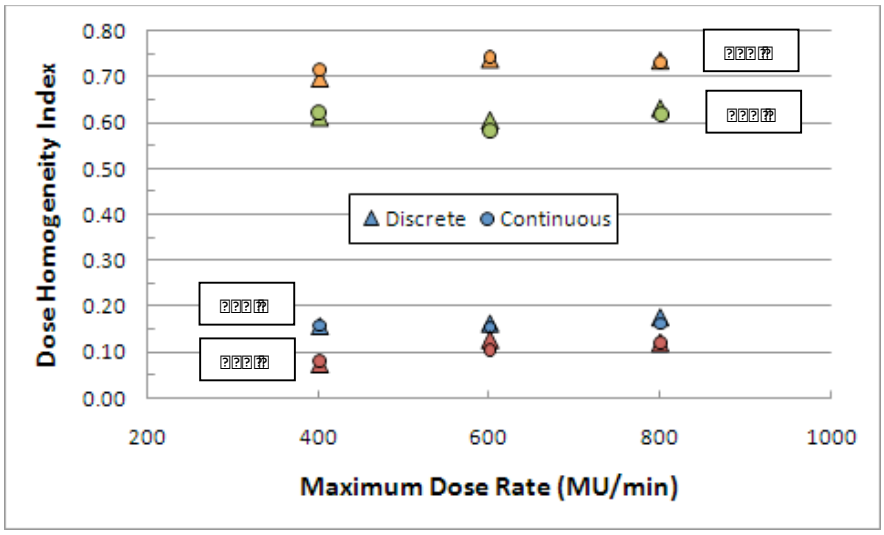

Figure 3-12. DHI for "Maximum Dose Rate" parameter: PTV 1 (78 Gy, blue), PTV 2 (61.6 Gy, red), PTV 3 (56 Gy, green), and PTV 4 (46.2 Gy, purple) of complex prostate case.

variable dose rates (triangles) are plotted for all PTVs. As the maximum dose rate increased from 400 MU/min to 800 MU/min, the DHI values for the phantom, simple prostate, and PTV1of the complex prostate varied by less than 0.02 for both continuously variable and discretely variable dose rates. Figure 3-12 shows DHI values for all PTVs of the complex prostate case. The DHI values for PTV2 for 400 MU/min differed by 0.052 and 0.023 from the

baseline DHI value (at 600 MU/min max) for discretely and continuously variable dose rates, respectively. The DHI values for PTV3 varied by 0.026 and 0.039 for discretely and continuously variable dose rates, respectively. The DHI for PTV4 varied by 0.042 and 0.029 for discretely and continuously variable dose rates, respectively. For all maximum dose rates and all treatment sites shown, the DHI for the continuously variable dose rates differed from the DHI for the discretely variable dose rates by less than 0.025. Only the DHI for PTV2 and PTV3 differed by more than 0.02 between continuous and discretely variable dose rates for the 600 MU/min maximum dose rate trials.

CI values for all maximum dose rates and all treatment sites are shown in Figure 3-13. CI for the phantom, simple prostate, and complex prostate cases varied by less than 0.02 over all maximum dose rates, both continuously and discretely variable. For all maximum dose rates and

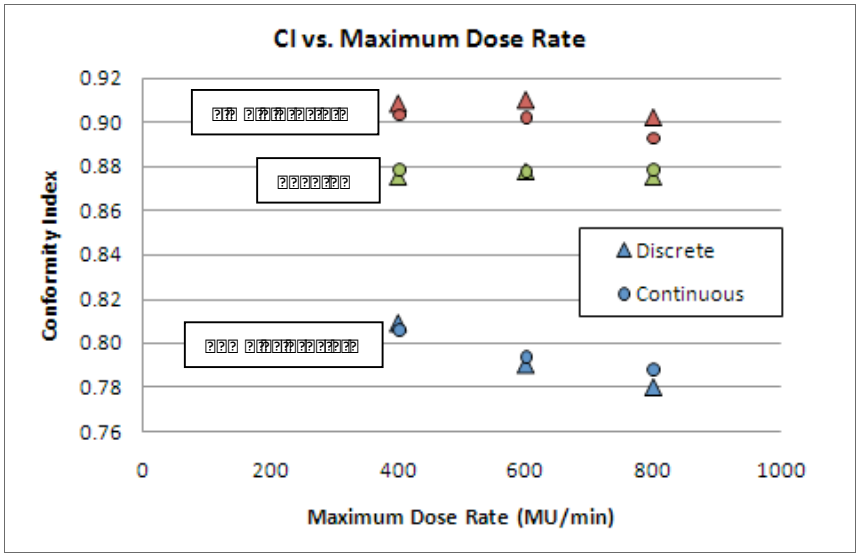

Figure 3-13. CI for "Maximum Dose Rate" parameter: phantom (green), simple prostate (red), and complex prostate (blue)cases.

all treatment sites shown, the CI for the continuously variable dose rates differed from the CI for the discretely variable dose rates by less than 0.02.

Normal tissue metrics for maximum dose rate variation are shown in Table 3-9. Dose values for all trials were normalized to the baseline plan. For a **given** maximum dose rate, the difference in dose values between continuously variable dose rates and discretely variable dose rates was less than 3% for most metrics across both treatment sites. The variation in dose to normal tissue metrics for **changing** maximum dose rates, however, was greater than 3% for every metric for the simple prostate case except for D_{25} of the bladder. For the complex prostate case, only D_{50} for the bladder (800 continuous) and D_{10} for the right femoral head (400 discrete) had greater than a 3% variation from the baseline value.

Table 3-9. Normal tissue metrics for Dose Rate variations for simple and complex prostate cases. All normal tissue dose metrics are normalized to baseline values.

Maximum Dose Rate	Norm %	Rectum		Bladder		Rt. Femoral Head		Lt. Femoral Head	
		D_{17}	D_{35}	D_{25}	D_{50}	D_{10}	$D_{max(1\%)}$	D_{10}	$D_{max(1\%)}$
Simple Prostate									
400 Disc*	95.7	1.053	1.058	1.021	1.033	0.897	0.922	0.971	0.997
400 Cont*	95.4	1.053	1.052	1.024	1.052	0.907	0.930	0.948	0.979
600 Disc	**95.4**	**1.000**	**1.000**	**1.000**	**1.000**	**1.000**	**1.000**	**1.000**	**1.000**
600 Cont	95.3	1.024	1.019	1.015	1.031	0.985	0.982	0.955	0.972
800 Disc	95.7	0.996	0.967	1.003	1.002	1.108	1.095	0.914	0.944
800 Cont	95.5	0.999	0.980	1.013	1.029	1.031	1.036	0.930	0.951
Complex Prostate									
400 Disc	95	1.014	1.016	0.995	1.015	1.031	0.999	1.012	0.997
400 Cont	95.3	1.020	1.022	1.010	1.018	1.028	1.007	1.000	0.987
600 Disc	**95**	**1.000**	**1.000**	**1.000**	**1.000**	**1.000**	**1.000**	**1.000**	**1.000**
600 Cont	95.3	0.997	0.991	0.996	0.989	0.986	0.976	0.996	0.983
800 Disc	94.9	1.006	1.027	1.026	0.996	1.002	0.979	0.991	0.996
800 Cont	94.9	1.009	1.005	0.773	1.230	1.016	0.988	1.002	0.986

* Disc = discretely variable dose rate, Cont = continuously variable dose rate

3.2.4 Maximum MLC Leaf Speed

Figures3-14and 3-15 show the effect of varying maximum leaf speed on DHI for the phantom, simple prostate, and complex prostate cases. As the maximum leaf speed was

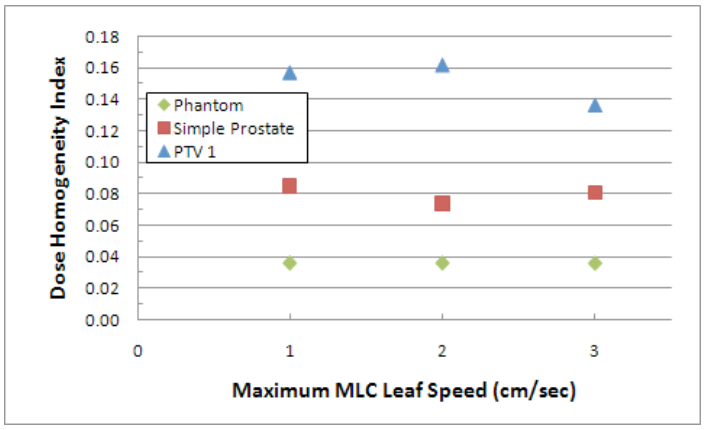

Figure 3-14. DHI for "Maximum MLC Leaf Speed" parameter: phantom (green), simple prostate (red), and PTV 1 (blue) of complex prostate case.

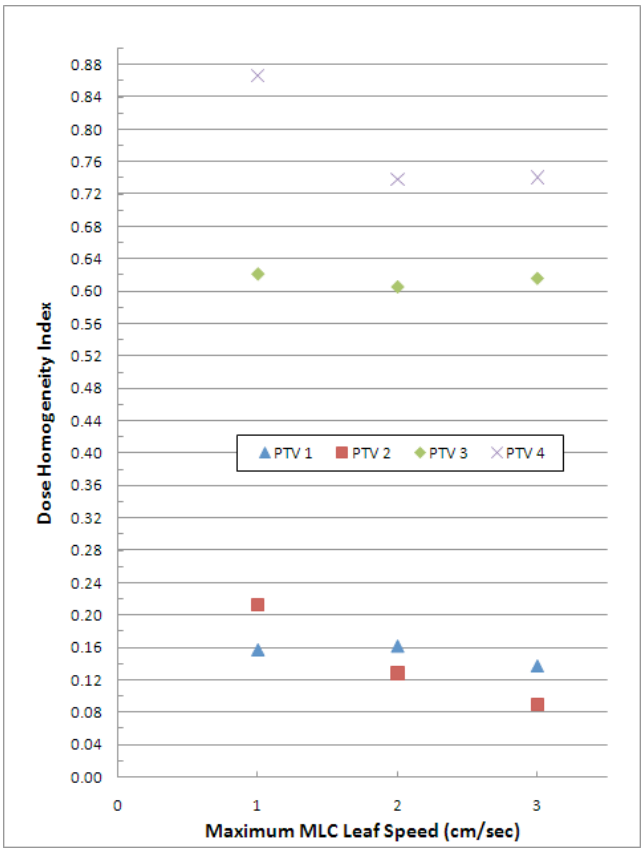

Figure 3-15. DHI for "Maximum MLC Leaf Speed" parameter: PTV 1 (78 Gy, blue), PTV 2 (61.6 Gy, red), PTV 3 (56 Gy, green), and PTV 4 (46.2 Gy, purple) of complex prostate case.

increased, the DHI for the phantom and simple prostate cases showed less than 0.02 variation while PTV 1 of the complex prostate case showed a variation of 0.025 in DHI values between

2cm/sec and 3cm/sec maximum leaf speed. DHI for PTV 1, PTV 2, and PTV 4 varied by 0.025, 0.085 and 0.128, respectively, and generally improved as maximum leaf speed increased. The DHI for PTV 3 varied by less than 0.02 among all maximum leaf speeds.

CI for maximum leaf speed variation is plotted in Figure 3-16. For the phantom and simple prostate cases, the CI varied by less than 0.02 across all maximum leaf speeds. For the complex prostate case, the CI variation was 0.022, and the CI improved as maximum leaf speed increased.

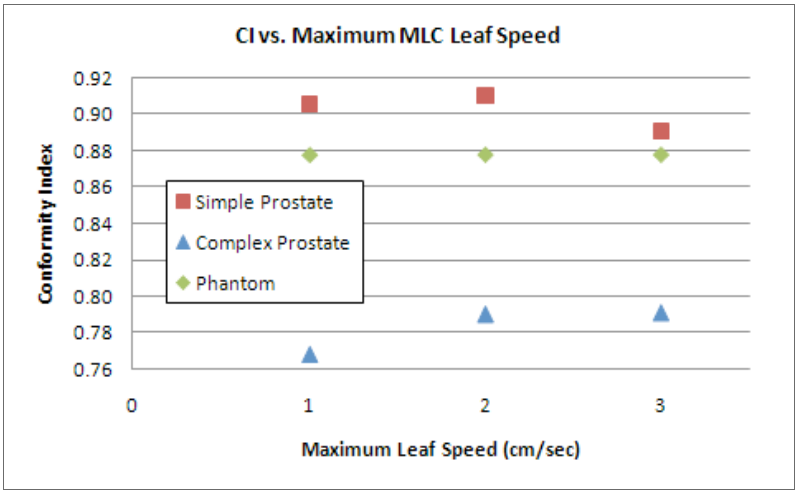

Figure 3-16. CI for "Maximum MLC Leaf Speed" parameter: phantom (green), simple prostate (red), and complex prostate (blue) cases.

Normal tissue metrics for changing maximum MLC leaf speed are shown in Table3-10. All dose values are normalized to the baseline trial. For the simple prostate case, metrics that exceeded a 3% variation in dose across all trials were D_{17} for the rectum, D_{25} for the bladder, and all metrics for the femoral heads. Metrics that exceeded 3% variation for the complex prostate case were D_{17} for the rectum, both bladder metrics, and all metrics for the femoral heads except for $D_{max(1\%)}$ for the right femoral head. With only 2 exceptions, metrics for the rectum and

bladder performed worse than the baseline plan for both 1 cm/sec and 3 cm/sec trials, while metrics for the femoral heads performed better.

Table 3-10. Normal tissue metrics for Maximum MLC Leaf Speed variations for simple and complex prostate cases. All normal tissue dose metrics are normalized to baseline values.

Max MLC Leaf Speed	Norm %	Rectum		Bladder		Rt. Femoral Head		Lt. Femoral Head	
		D_{17}	D_{35}	D_{25}	D_{50}	D_{10}	$D_{max(1\%)}$	D_{10}	$D_{max(1\%)}$
Simple Prostate									
1 cm/sec	95.9	1.031	1.022	1.085	1.007	0.937	0.945	0.963	0.958
2 cm/sec	**95.4**	**1.000**	**1.000**	**1.000**	**1.000**	**1.000**	**1.000**	**1.000**	**1.000**
3 cm/sec	95.9	1.027	1.016	1.050	1.030	0.994	0.982	0.961	0.972
Complex Prostate									
1 cm/sec	95.3	1.030	1.029	1.073	1.066	1.007	0.985	0.975	0.955
2 cm/sec	**95**	**1.000**	**1.000**	**1.000**	**1.000**	**1.000**	**1.000**	**1.000**	**1.000**
3 cm/sec	95	0.995	0.999	1.014	1.006	0.951	0.994	0.965	0.942

3.2.5 MLC Leaf Size

DHI and CI results for varying MLC size are shown in Table 3-11. DHI values for the two leaf sizes for the phantom and simple prostate cases differed by less than 0.02. The variation in DHI for PTV1, PTV2, and PTV4 of the complex prostate case was also less than 0.02, while the DHI value for PTV3 was 0.043 lower for 1cm leaf size.

The difference in CI values for the two leaf sizes for phantom and simple prostate cases was less than 0.02. The CI value for PTV1 was 0.03 greater for the 5mm leaf size.

Table 3-11. DHI and CI values for MLC Leaf Size (PTV 1: 78Gy, PTV 2: 61.6Gy, PTV 3: 56Gy, PTV 4: 46.2Gy).

Dose Homogeneity Index

Leaf Size	Phantom	Simple Prostate	Complex Prostate			
			PTV 1	PTV 2	PTV 3	PTV 4
1 cm	**0.0358**	**0.0736**	**0.1619**	**0.1274**	**0.6050**	**0.7379**
5mm	0.0426	0.0768	0.1473	0.1068	0.6482	0.7091

Conformity Index

Leaf Size	Phantom	Simple Prostate	Complex Prostate
1 cm	**0.8777**	**0.9106**	**0.7900**
5mm	0.8634	0.8946	0.8196

Normal tissue metrics for the different MLC leaf sizes are shown in Table 3-12. For the simple prostate case, dose metrics for the rectum and D_{25} for the bladder were less than 3%

Table 3-12. Normal tissue metrics for MLC Leaf Size variation for simple and complex prostate cases. All normal tissue dose metrics are shown in cGy.

Leaf Size	Norm %	Rectum		Bladder		Rt. Femoral Head		Lt. Femoral Head	
		D_{17}	D_{35}	D_{25}	D_{50}	D_{10}	$D_{max(1\%)}$	D_{10}	$D_{max(1\%)}$
Simple Prostate									
1 cm	**95.4**	**3893**	**4420**	**1927**	**3702**	**3927**	**3855**	**4248**	**4248**
5 mm	95.6	4014	4541	1965	3373	3800	3476	3815	4147
Complex Prostate									
1 cm	**95**	**6666**	**5066**	**6054**	**4811**	**4250**	**4748**	**4477**	**4868**
5 mm	94.8	6627	4960	5810	4543	3937	4383	4239	4628

different between the two trials. All other metrics differed by up to 10% and performed better for the 5mm leaf size. For the complex prostate case, all metrics differed by more than 3% between the two trials except for D_{17} of the rectum. The greatest discrepancy was about 8% for both metrics for the right femoral head. Dose metrics for the complex prostate case performed better for the 5mm leaf size trial.

3.2.6 Maximum MU/degree

Two trials were run to investigate the effect of changing the maximum MU/degree: 100 MU/deg and 1 MU/deg. DHI and CI results are shown in Table 3-13. Phantom and complex

Table 3-13. DHI and CI values for Maximum MU/degree (PTV 1: 78Gy, PTV 2: 61.6Gy, PTV 3: 56Gy, PTV 4: 46.2Gy).

Dose Homogeneity Index

MU/degree	Phantom	Simple Prostate	Complex Prostate			
			PTV 1	PTV 2	PTV 3	PTV 4
100 MU/deg	**0.0358**	**0.0736**	**0.1619**	**0.1274**	**0.6050**	**0.7379**
1 MU/deg	0.0358	0.0728	0.1619	0.1274	0.6050	0.7379

Conformity Index

MU/degree	Phantom	Simple Prostate	Complex Prostate
100 MU/deg	**0.8777**	**0.9106**	**0.7900**
1 MU/deg	0.8777	0.9127	0.7900

prostate cases showed identical resulting plans for this parameter, and the simple prostate case varied less than 0.02 for both DHI and CI. Allowing only 1 MU/degree would result in a plan with a maximum of 360 MU for a 360 degree total arc length. All resulting plans for 1MU/deg trials exceeded 360 MU. The control point data was reviewed for these trials, and hand calculations for MU/degree verified that the treatment planning system ignored the 1 MU/deg limitation.

Normal tissue metrics for MU/degree trials are shown in Table 3-14. Values for the simple prostate case varied less than 3% between trials.

Table 3-14.Normal tissue metrics for Maximum MU/degree variations for simple and complex prostate cases. All dose values are shown in cGy.

MU/degree	Norm. %	Rectum		Bladder		Rt. Femoral Head		Lt. Femoral Head	
		D_{17}	D_{35}	D_{35}	D_{50}	D_{10}	$D_{max(1\%)}$	D_{10}	$D_{max(1\%)}$
Simple Prostate									
100 MU/deg	**95.4**	**5297**	**3893**	**4420**	**1927**	**3702**	**3927**	**3855**	**4248**
1 MU/deg	95.5	5381	3930	4405	1963	3647	3877	3760	4147
Complex Prostate									
100 MU/deg	**95**	**6666**	**5066**	**6054**	**4811**	**4250**	**4748**	**4477**	**4868**
1 MU/deg	95	6666	5066	6054	4811	4250	4748	4477	4868

3.3 Planning Parameters

3.3.1 Beam Energy

Figures 3-17 and 3-18 are plots of the resulting DHI for energies of 6MV, 10MV, and 15MV. DHI values for the phantom and simple prostate cases varied by less than 0.02 for all three energies. The difference in DHI for PTV1 between the 6MV trial and the 15MV trial was 0.038, and the DHI performed better for lower energies. The differences in DHI for PTV2,

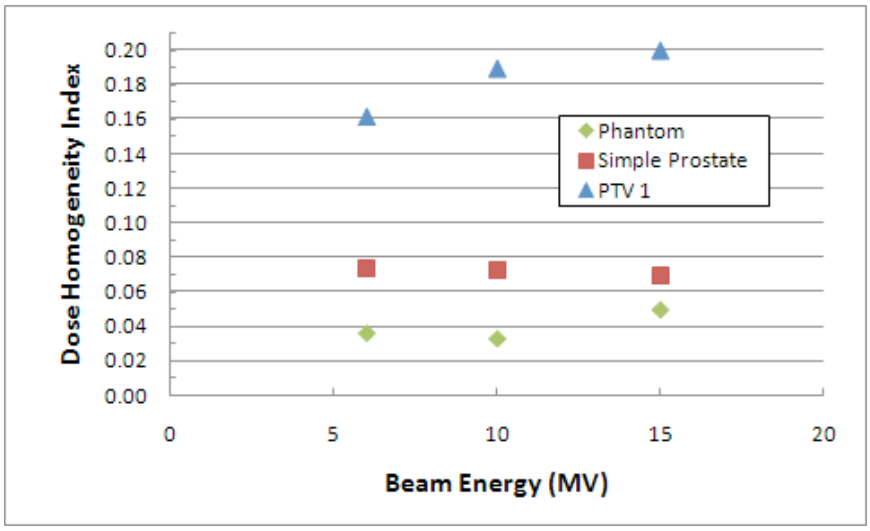

Figure 3-17. DHI for "Beam Energy" parameter: phantom (green), simple prostate (red), and PTV 1 (blue) of complex prostate case.

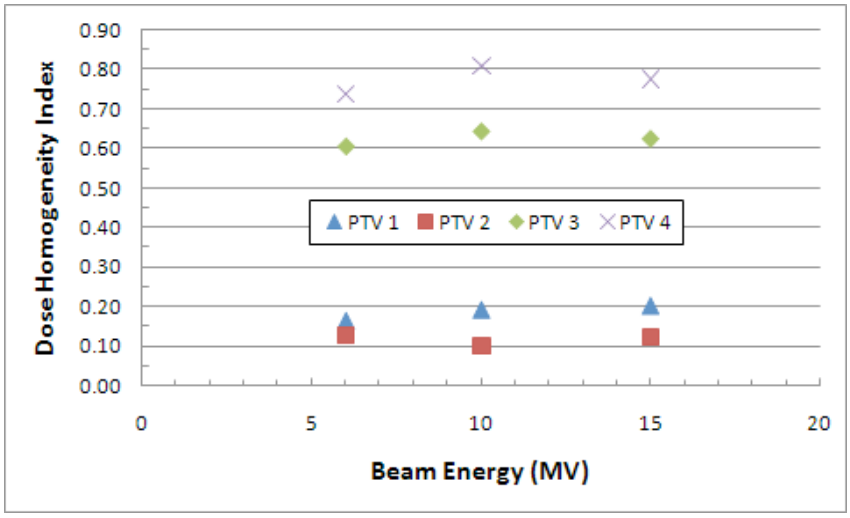

Figure 3-18. DHI for "Beam Energy" parameter: PTV 1 (78 Gy, blue), PTV 2 (61.6 Gy, red), PTV 3 (56 Gy, green), and PTV 4 (46.2 Gy, purple) of complex prostate case.

PTV3, and PTV4 (between the baseline DHI value and the DHI value with greatest variation from the baseline value) were 0.028, 0.038, and 0.071, respectively, and there was no consistent trend for DHI performance as beam energy increased.

The CI for all treatment sites and all energies is shown in Figure 3-19. The variation in CI across the three beam energies was 0.056, 0.022, and 0.07 for the phantom case, the simple prostate case, and the complex prostate case, respectively. There was no common trend for target conformity as beam energy increased.

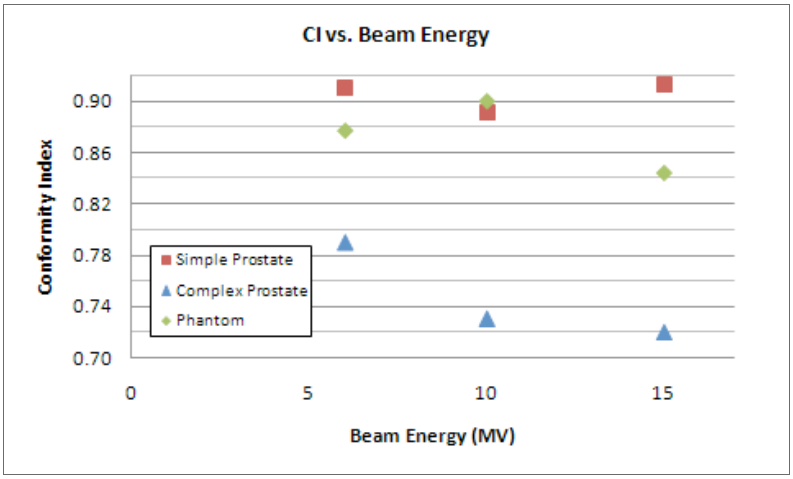

Figure 3-19. CI for "Beam Energy" parameter: phantom (green), simple prostate (red), and complex prostate (blue) cases.

Table 3-18. Normal tissue metrics for Beam Energy variations for simple and complex prostate cases. All normal tissue dose metrics are normalized to baseline values.

Beam Energy	Norm. %	Rectum		Bladder		Rt. Femoral Head		Lt. Femoral Head	
		D_{17}	D_{35}	D_{25}	D_{50}	D_{10}	$D_{max(1\%)}$	D_{10}	$D_{max(1\%)}$
Simple Prostate									
6 MV	**95.4**	**1.000**	**1.000**	**1.000**	**1.000**	**1.000**	**1.000**	**1.000**	**1.000**
10 MV	96.1	0.986	0.915	1.036	1.020	1.078	1.091	1.038	1.034
15 MV	96.2	1.026	1.000	1.042	1.118	1.007	1.028	1.011	1.014
Complex Prostate									
6 MV	**95**	**1.000**	**1.000**	**1.000**	**1.000**	**1.000**	**1.000**	**1.000**	**1.000**
10 MV	95.2	1.000	1.017	1.019	1.016	1.058	1.045	0.987	0.978
15 MV	95.2	1.011	1.035	1.008	0.995	1.120	1.060	1.017	1.016

Normal tissue metrics for the three beam energies are shown in Table 3-18 for the simple and complex prostate cases, normalized to the baseline plan. With few exceptions, the higher energies performed worse for sparing normal tissue, and most metrics had greater than 3% variation across all energies for both treatment sites.

3.3.2 Arc Length

DHI for varying arc lengths are shown in Figure 3-20 for the phantom, simple prostate, and PTV1 of the complex prostate. DHI for varying arc lengths are shown in Figure 3-21 for all PTVs of the complex prostate case. The DHI improved as the arc length increased for all PTVs. The larger arc lengths involved more control points, which allowed for better modulation of the dose to the target volume. Pinnacle version 8.1y does not have double arc optimization capabilities,so 360 deg was the largest arc studied here. From 60 to 180 degrees total arc length, there is an extreme improvement in DHI as arc length is increased. Between 180 degrees and 360 degrees total arc length, DHI continues to improve, but the rate of improvement is not as severe. This is due to exit dose generated by the photon radiation. The entire PTV is treated with a 180-degree arc, but a 360-degree arc allows for improvement in dose homogeneity.

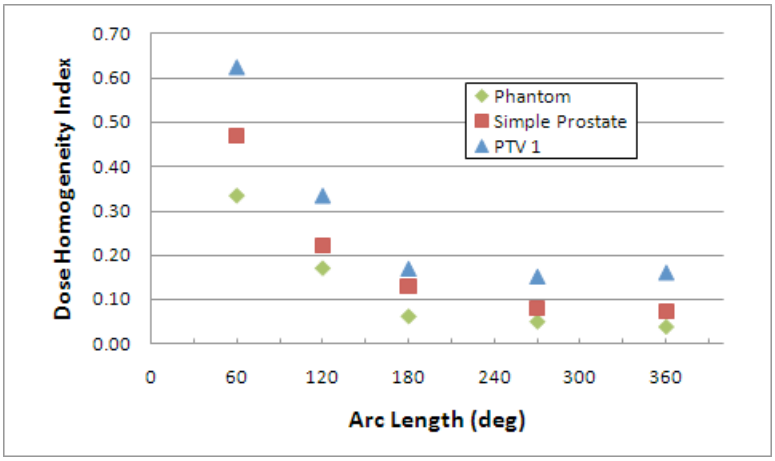

Figure 3-20. DHI for "Arc Length" parameter: phantom (green), simple prostate (red), and PTV 1 (blue) of complex prostate case.

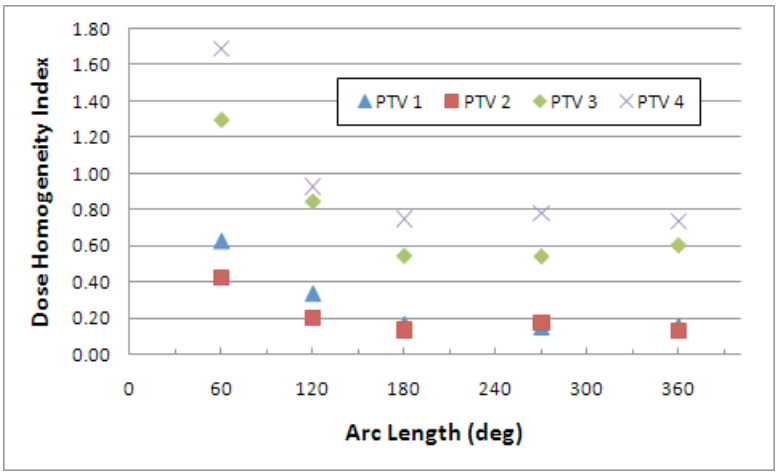

Figure 3-21. DHI for "Arc Length" parameter: PTV 1 (78 Gy, blue), PTV 2 (61.6 Gy, red), PTV 3 (56 Gy, green), and PTV 4 (46.2 Gy, purple) of complex prostate case.

The CI for arc length trials are plotted in Figure 3-22. As expected, the CI also improved as arc length increased because more control points allowed for better conformity of the prescription dose to the PTV. The rate of improvement in CI also declined at 180 degrees total arc length.

Normal tissue metrics for arc length variations are shown in Figure 3-23. For the smaller arc lengths, normal tissue sparing depended greatly on how the arc was oriented. With the

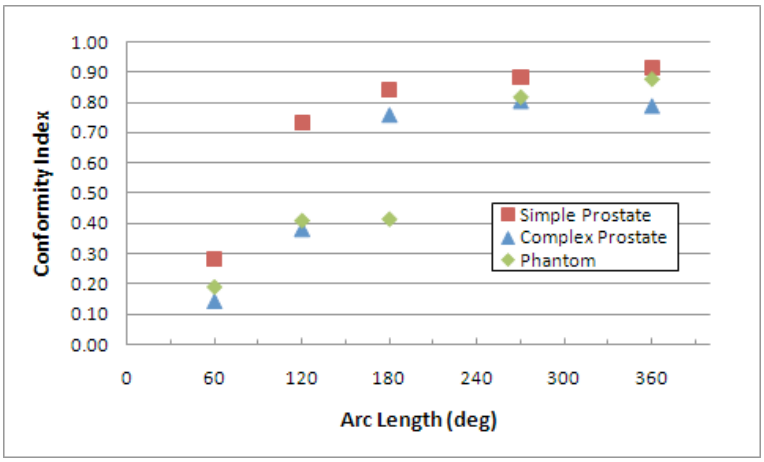

Figure 3-22. CI for "Arc Length" parameter: phantom (green), simple prostate (red), and complex prostate (blue) cases.

exception of the femoral heads, which were partly spared for smaller arcs, normal tissue sparing improved as arc length increased.

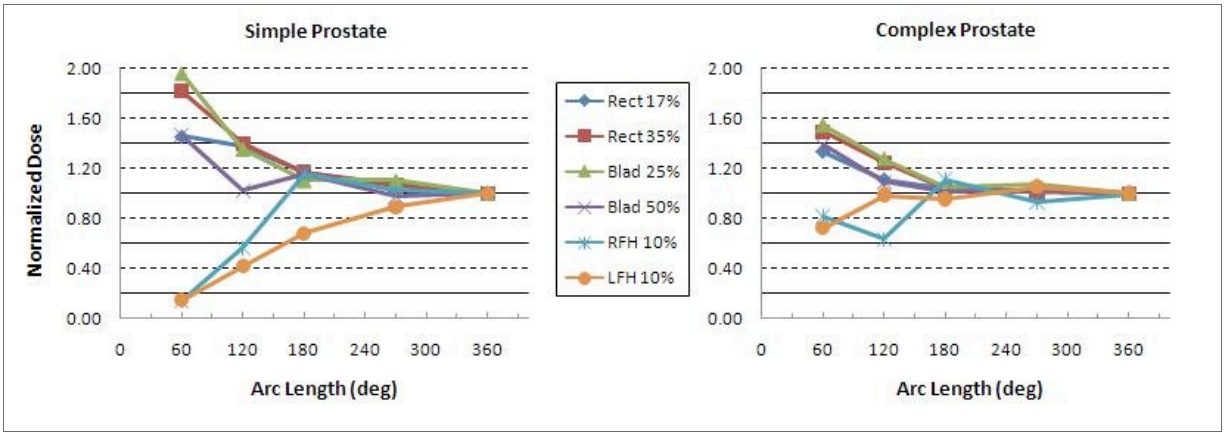

Figure 3-23.Normal tissue metrics for "Arc Length" parameter for simple prostate and complex prostate cases. All doses normalized to dose values for the baseline trial (360 deg).

3.3.3 Collimator Angle

The collimator angle was varied from 0 to 90 degrees for all treatment sites. For the phantom case, the baseline collimator angle was 90 degrees. For both the simple and complex prostate cases, the baseline collimator angle was 0 degrees. Figures 3-24 and 3-25 show the DHI values for all three treatment sites for all collimator angles studied. The DHI variation across all collimator angles for the phantom case was less than 0.02. The greatest variation in DHI values all collimator angles for the simple prostate case was 0.027. For the complex prostate case, changing collimator angle had the biggest effect on the DHI for PTV4, where DHI values varied by 0.294 from a collimator angle of 0 degrees to a collimator angle of 90 degrees. PTV1, PTV2, and PTV3 had DHI variations of 0.047, 0.061, and 0.062, respectively.

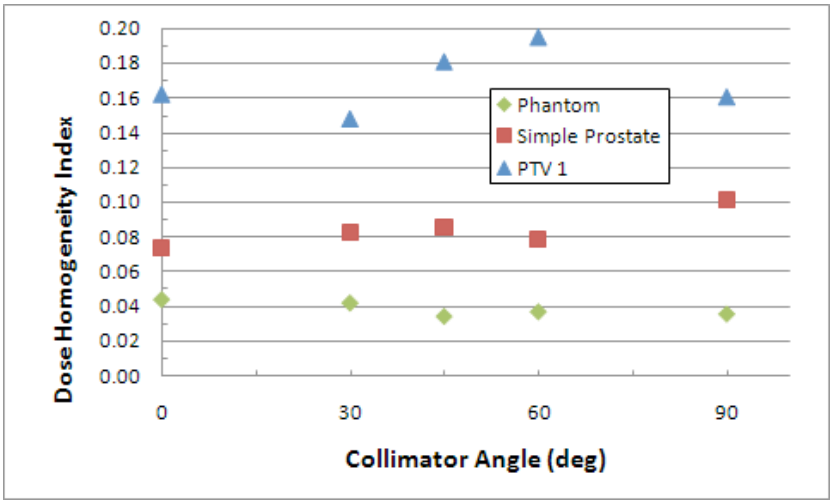

Figure 3-24. DHI for "Collimator Angle" parameter: phantom (green), simple prostate (red), and PTV 1 (blue) of complex prostate case.

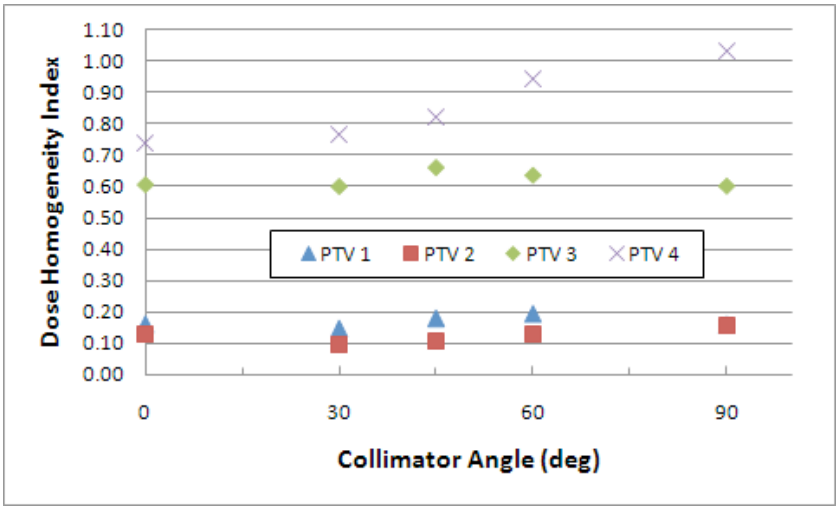

Figure 3-25. DHI for "Collimator Angle" parameter: PTV 1 (78 Gy, blue), PTV 2 (61.6 Gy, red), PTV 3 (56 Gy, green), and PTV 4 (46.2 Gy, purple) of complex prostate case.

CI for collimator angle variations are shown in Figure 3-26. The CI values for the phantom and the simple prostate cases varied across all collimator angles by 0.059 and 0.069, respectively. The largest variation in CI values was 0.127 for the PTV1 of the complex prostate case.

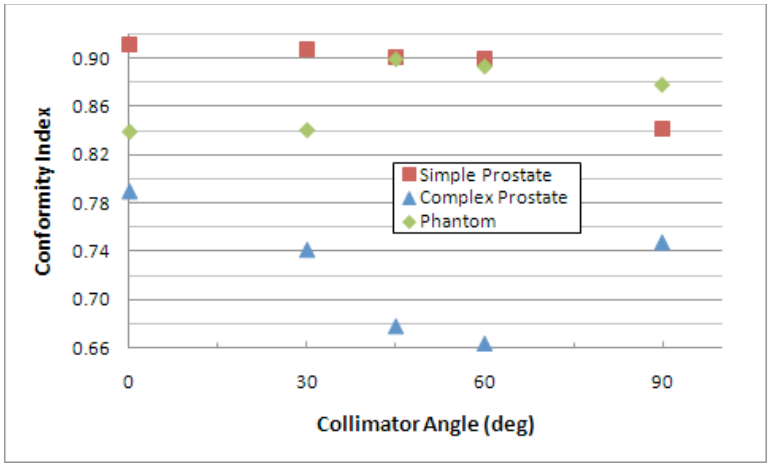

Figure 3-26. CI for "Collimator Angle" parameter: phantom (green), simple prostate (red), and complex prostate (blue) cases.

Normal tissue metrics for the simple and complex prostate cases are plotted against collimator angle in Figure 3-27. Metrics for the simple prostate case generally varied more than metrics for the complex prostate case. The simple prostate case had fewer optimization goals and constraints than the complex prostate case, allowing the optimization more room to diverge from the baseline plan. For the simple prostate case, D_{50} for the bladder varied over 40% by changing the collimator from 0 degrees to 90 degrees. All other metrics, except for the left femoral head varied between 17% and 25% from 0 to 90 degrees. The most variation from the

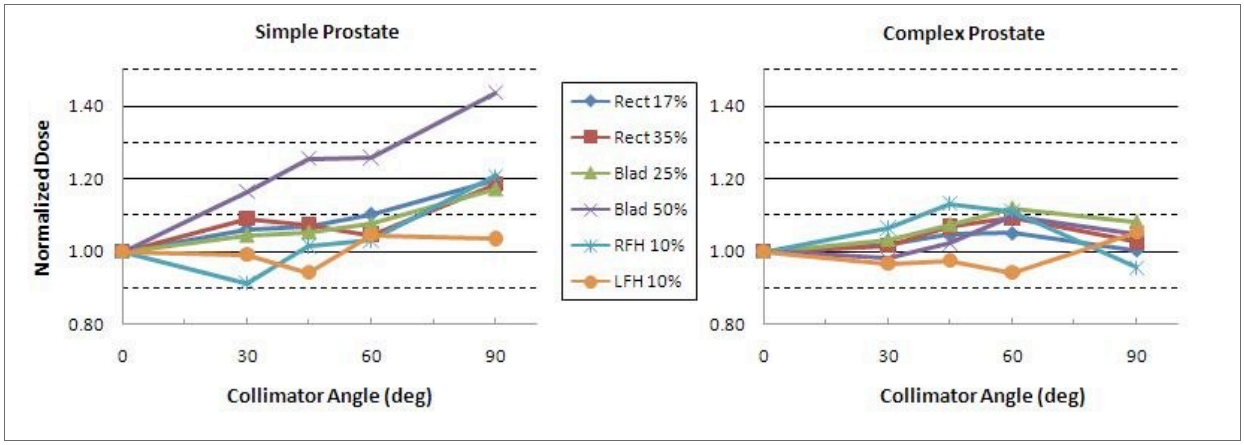

Figure 3-27. Normal tissue metrics for "Collimator Angle" parameter for simple prostate and complex prostate cases. All doses normalized to dose values for the baseline trial (360 deg).

baseline plan for the complex prostate case was 12% for D_{25} for the bladder with a collimator angle of 60 degrees.

3.3.4 Dose Grid Resolution

Trials were run for 0.3cm, 0.4cm, and 0.5cm resolution. Figures 3-28 and 3-29 show DHI values for the phantom, simple prostate, and complex prostate cases. For the complex prostate case, only dose grid resolutions of 0.4cm and 0.5cm were used due to software failures

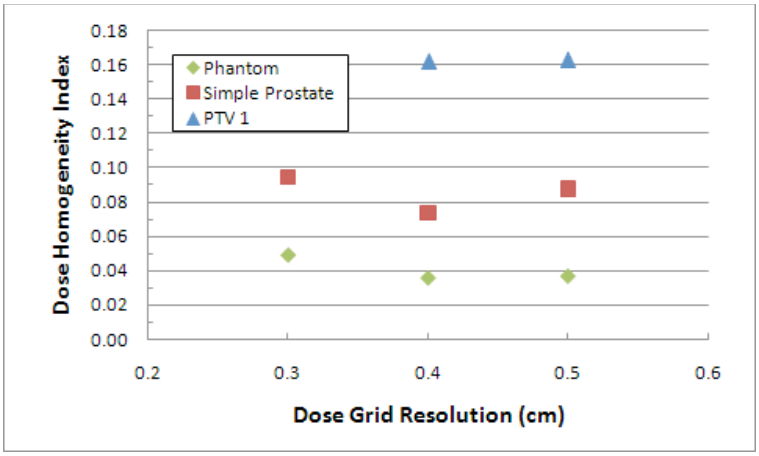

Figure 3-28. DHI for "Dose Grid Resolution" parameter: phantom (green), simple prostate (red), and PTV 1 (blue) of complex prostate case.

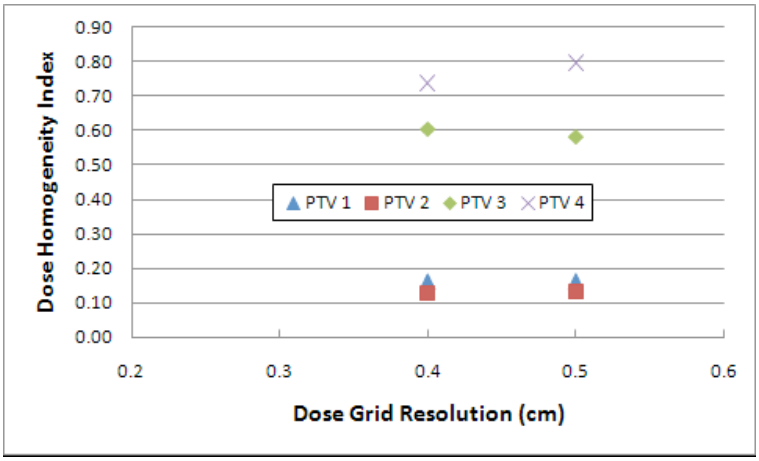

Figure 3-29. DHI for "Dose Grid Resolution" parameter: PTV 1 (78 Gy, blue), PTV 2 (61.6 Gy, red), PTV 3 (56 Gy, green), and PTV 4 (46.2 Gy, purple) of complex prostate case.

of the treatment planning system. The variation in DHI values across all dose grid resolutions for the phantom case was less than 0.02. The variation in DHI values for the simple prostate case was only 0.021. The difference in DHI values between both dose grid resolutions for PTV1 and PTV2 of the complex prostate case was less than 0.02, while the difference in DHI values for PTV3 and PTV4 between both dose grid resolutions was 0.023 and 0.060, respectively.

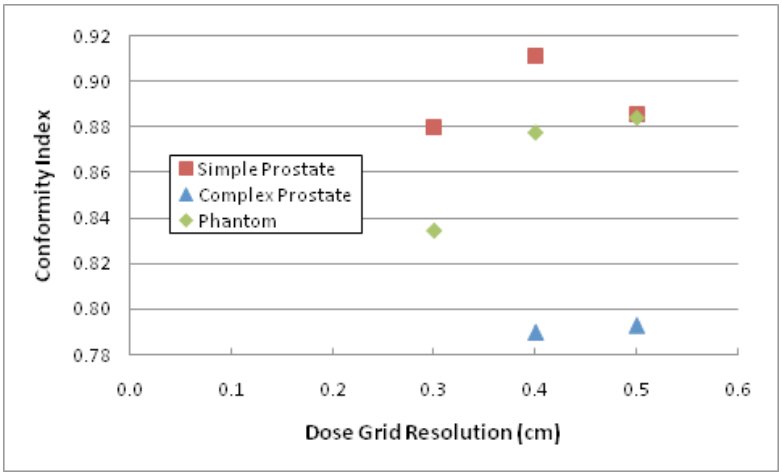

Figure 30.CI for "Dose Grid Resolution" parameter: phantom (green), simple prostate (red), and complex prostate (blue) cases.

Table 3-19. Normal tissue metrics for Dose Grid Resolution variations for simple and complex prostate cases. All normal tissue dose metrics are normalized to baseline values (0.4cm).

Dose Grid Resolution	Norm %	Rectum		Bladder		Rt. Femoral Head		Lt. Femoral Head	
		D_{17}	D_{35}	D_{25}	D_{50}	D_{10}	$D_{max(1\%)}$	D_{10}	$D_{max(1\%)}$
Simple Prostate									
0.3 cm	95.3	0.970	0.968	1.034	1.070	0.928	0.979	0.967	0.965
0.4 cm	**95.4**	**1.000**	**1.000**	**1.000**	**1.000**	**1.000**	**1.000**	**1.000**	**1.000**
0.5 cm	95.4	1.054	1.062	1.056	1.061	0.940	1.015	0.932	0.935
Complex Prostate									
0.4 cm	**95**	**1.000**	**1.000**	**1.000**	**1.000**	**1.000**	**1.000**	**1.000**	**1.000**
0.5 cm	95	1.013	1.001	1.036	1.013	0.930	0.933	0.832	0.907

The CI for all treatment sites is plotted against the dose grid resolution in Figure 3-30. The variation in CI values was 0.050 for the phantom case and 0.031for the simple prostate case.

A dose grid resolution of 0.3cm provided the worst CI for both the phantom and simple prostate cases. The two CI values for the complex prostate case differed by less than 0.02.

Normal tissue metrics for dose grid resolution variation are shown in Table 3-19, normalized to the baseline values. All metrics for the simple prostate case and most metrics for the complex prostate case showed greater than 3% variation from the baseline values. The dose to both rectum metrics and to D_{50} of the bladder varied by less than 3% between the 0.5cm trial and the baseline trial for the complex prostate case.

3.3.5 Final Gantry Spacing

The setting for final gantry spacing determines the spacing of control points around the final arc. The options for final gantry spacing were 2, 3, 4, or 6 degrees. It is recommended in the literature to start with a spacing of 4 degrees (RaySearch Laboratories, 2009). DHI values are shown for all spacing options for all treatment sites in Figures 3-31 and 3-32. Trials with 2

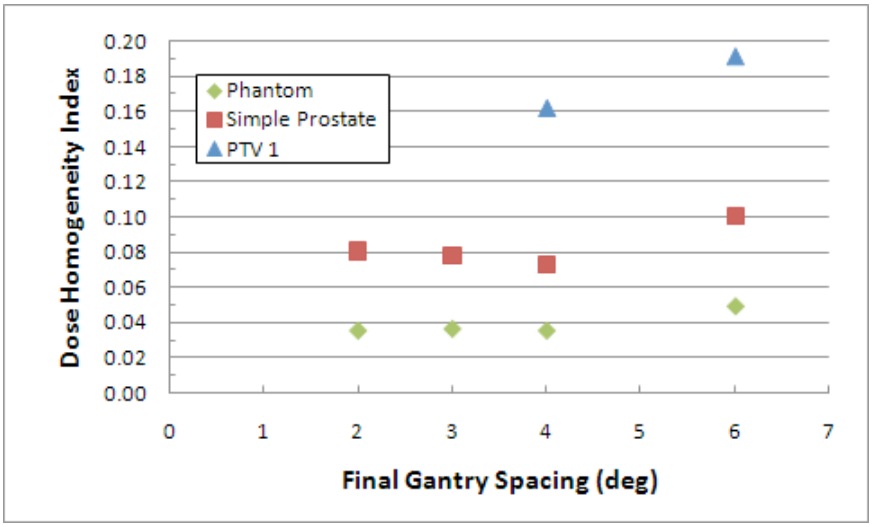

Figure 3-31. DHI for "Final Gantry Spacing" parameter: phantom (green), simple prostate (red), and PTV 1 (blue) of complex prostate case.

and 3 degrees final spacing could not be run for the complex prostate case due to software failures of the treatment planning system. For the phantom case, the variation in DHI values across all final gantry spacing options was less than 0.02. The variation in DHI values for the simple prostate case was less than 0.02 for 2, 3, and 4 degrees final gantry spacing, but for 6 degree final gantry spacing, the DHI increased by 0.027 from the baseline value (4 degrees). Similarly, the DHI value for 6 degree final gantry spacing for PTV1 of the complex prostate case was 0.030 higher than the baseline, and the DHI value for 6 degree final gantry spacing for PTV3 was 0.028. The difference in DHI values for PTV2 and PTV4 was less than 0.02 between 4 and 6 degrees final gantry spacing trials.

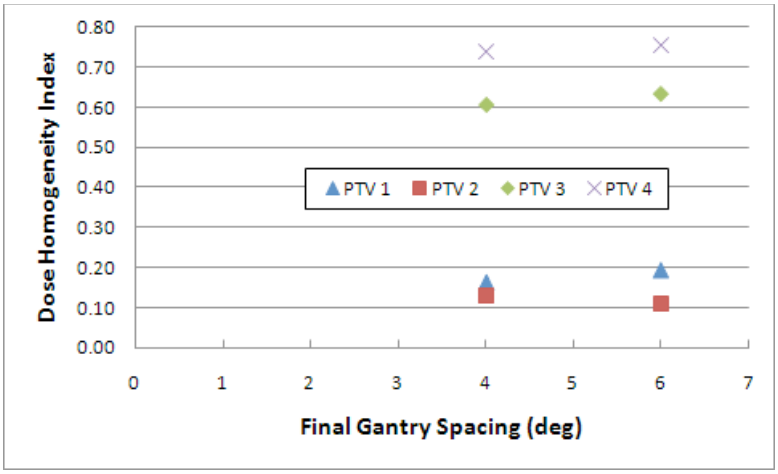

Figure 3-32. DHI for "Final Gantry Spacing" parameter: PTV 1 (78 Gy, blue), PTV 2 (61.6 Gy, red), PTV 3 (56 Gy, green), and PTV 4 (46.2 Gy, purple) of complex prostate case.

The CI values for final gantry spacing trials are shown in Figure 3-33. Similar to the DHI plots, the variation in CI values for the phantom and simple prostate cases remained less than 0.02 for 2, 3, and 4 degree final gantry spacing. The difference in CI values between 4- degree final gantry spacing and 6-degree final gantry spacing was 0.049 for the phantom case, 0.032 for the simple prostate case, and 0.117 for the complex prostate case. Target conformity was worst

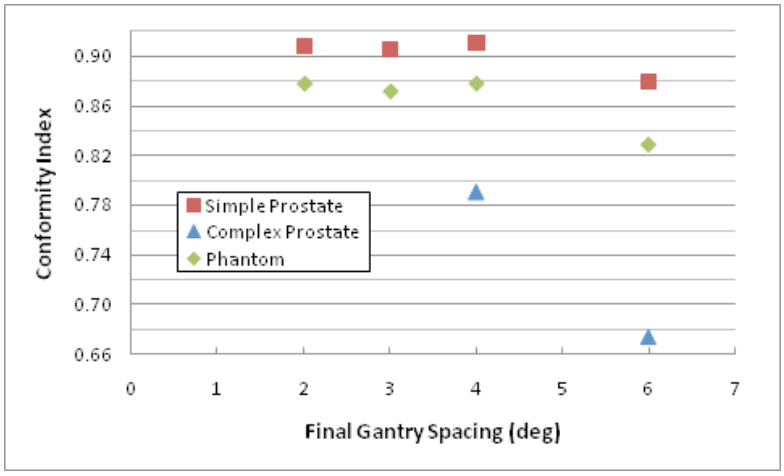

Figure 3-33. CI for "Final Gantry Spacing" parameter: phantom (green), simple prostate (red), and complex prostate (blue) cases.

for 6 degree final gantry spacing for all treatment sites, most dramatically for the complex prostate.

All normal tissue metrics for final gantry spacing variations are shown in Table 3-20, normalized to the baseline values (4 degrees). For the simple prostate case, 6-degree final gantry spacing, all metrics showed greater than 3% difference from the baseline plan except $D_{max(!\%)}$ for both femoral heads. The only other metrics that showed greater than 3% difference from the

Table 3-20. Normal tissue metrics for Final Gantry Spacing variations for simple and complex prostate cases. All normal tissue dose metrics are normalized to baseline values (4 deg).

Final Gantry Spacing	Norm %	Rectum		Bladder		Rt. Femoral Head		Lt. Femoral Head	
		D_{17}	D_{35}	D_{25}	D_{50}	D_{10}	$D_{max(1\%)}$	D_{10}	$D_{max(!\%)}$
Simple Prostate									
2 deg	95.9	0.993	0.965	0.997	1.024	1.020	1.022	1.005	1.034
3 deg	95.5	1.003	0.978	0.992	0.983	0.985	0.997	0.981	1.009
4 deg	**95.4**	**1.000**	**1.000**	**1.000**	**1.000**	**1.000**	**1.000**	**1.000**	**1.000**
6 deg	95.2	1.061	1.048	1.040	0.929	0.935	0.980	0.955	0.997
Complex Prostate									
4 deg	**95**	**1.000**	**1.000**	**1.000**	**1.000**	**1.000**	**1.000**	**1.000**	**1.000**
6 deg	95	1.031	1.064	1.012	1.019	1.071	1.016	1.023	0.999

baseline values for the simple prostate case were D_{35} of the rectum, and $D_{max(!\%)}$ of the left femoral head for 2 degree final gantry spacing. For the complex prostate case, 6 degree final gantry spacing, both rectum metrics and D_{10} of the right femoral head showed greater than 3% difference from the baseline values.

3.3.6 Maximum Delivery Time

The data collected in this study for maximum delivery time was based on the user-requested maximum delivery time, not the actual delivery time estimated by Pinnacle after optimization. Table 3-21 shows both the input maximum delivery times (user-requested) and estimated delivery times for the three treatment sites. Trials were run for all treatment sites with 60-second, 120-second, and 240-second maximum delivery times, along with intermediate maximum delivery times that were different for each treatment geometry.

Table 3-21. Input maximum delivery time and estimated delivery time for all trials, all treatment sites.

Phantom		**Simple Prostate**		**Complex Prostate**	
Input (sec)	Est. Delivery (sec)	Input (sec)	Est. Delivery (sec)	Input (sec)	Est. Delivery (sec)
20	60	20	60	--	--
45	60	--	--	--	--
60	60	60	60	60	64
--	--	90	88	--	--
120	**98**	**120**	**110**	**120**	**119**
--	--	--	--	150	143
240	194	240	211	240	194

The data for DHI values for different maximum delivery times is shown in Figures 3-34 and 3-35. The phantom case resulted in identical plans for both 20-second maximum delivery time and 45-second maximum delivery time. The actual estimated delivery time for both plans was approximately 60 seconds, indicating that the 20-second and 45-second limitations were rejected by the treatment planning system for those trials. The variation in DHI values for all other trials for the phantom case were within 0.02 of the baseline DHI value (120 seconds). The

variation in DHI values for the simple prostate case remained within 0.02 of the baseline DHI values for 20-second, 60-second, and 90-second trials. The DHI value for the 240-second trial for the simple prostate case, however, was 0.028 greater than the DHI for the baseline trial. For the simple prostate case, the longest maximum delivery time requested resulted in worse dose homogeneity across the PTV. DHI values for the 60-second and 150-second trials for PTV1 of the complex prostate case were within 0.02 of the baseline DHI value, but the DHI value for the 240-second trial was 0.028 less than the baseline value. For PTV1 of the complex prostate case,

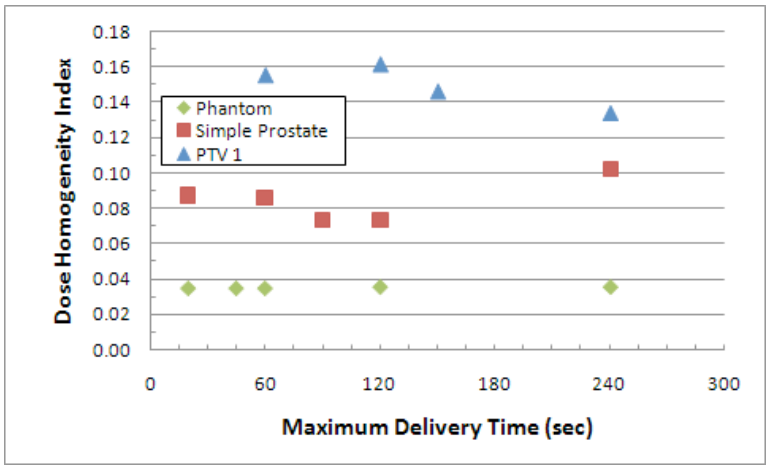

Figure 3-34. DHI for "Maximum Delivery Time" parameter: phantom (green), simple prostate (red), and PTV 1 (blue) of complex prostate case.

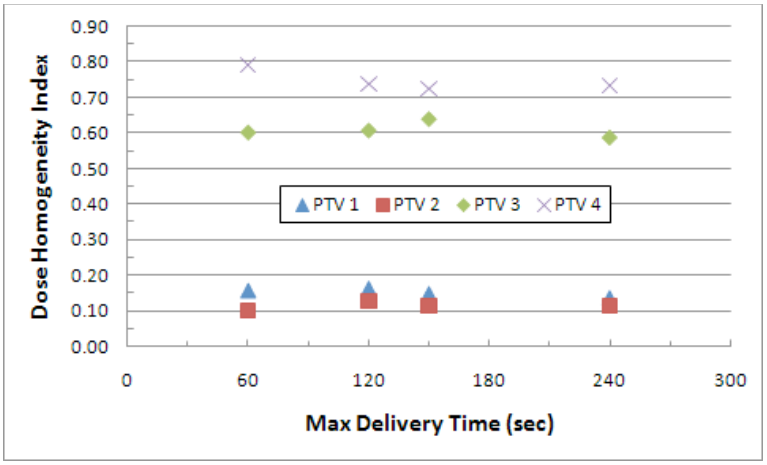

Figure 3-35. DHI for "Maximum Delivery Time" parameter: PTV 1 (78 Gy, blue), PTV 2 (61.6 Gy, red), PTV 3 (56 Gy, green), and PTV 4 (46.2 Gy, purple) of complex prostate case.

the longer maximum delivery time resulted in better dose homogeneity across the target volume. DHI values for all PTVs of the complex prostate case are plotted in Figure 3-35. The DHI for the 60-second trial for PTV2 differed by 0.028 from the baseline trial, while DHI values for all other trials for PTV2 were within 0.02 of the baseline DHI value. For PTV3, the 150-second trial resulted in a DHI value 0.032 greater than the baseline DHI value. DHI values for PTV4 were mostly within 0.02 variation from the baseline plan, but the DHI for the 60-second trial was 0.051greater.

The CI as a function of maximum delivery time is shown in Figure 3-36. All trials for the phantom case resulted in a variation of CI values of less than 0.02 from the baseline CI value (120 seconds). CI values for the simple prostate case were within 0.02 of the baseline value for the 20-second, 60-second, and 90-second trials, but the CI value for the 240-second trial was 0.036 lower than the CI value for the baseline trial. All CI values for the complex prostate case were within 0.02 of the baseline CI value.

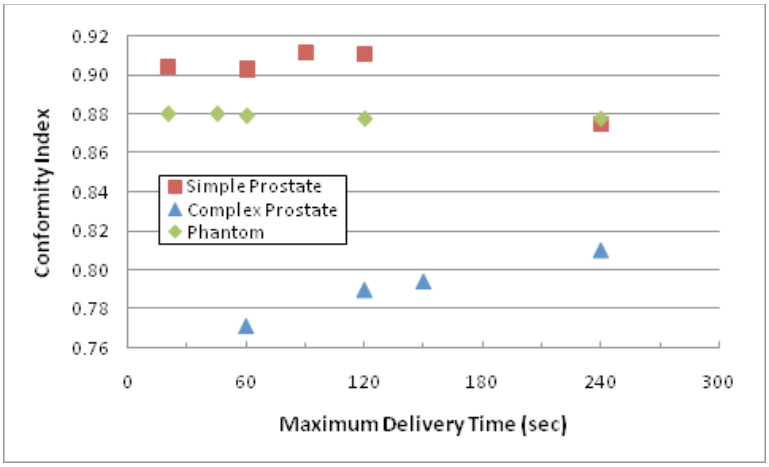

Figure 3-36. CI for "Maximum Delivery Time" parameter: phantom (green), simple prostate (red), and complex prostate (blue) cases.

Normal tissue metrics for varying maximum delivery time are plotted in Figure3-37, normalized to the baseline trial. For the simple prostate case, the right femoral head received

greater dose as the maximum delivery time increased, but both rectum metrics received less dose for greater maximum delivery times. The left femoral head showed no trend as requested delivery timed increased, but performed worst for the baseline trial. The bladder metrics showed no consistent trend, but were lowest for the baseline trial. For the complex prostate case, all normal tissues generally performed better for longer maximum delivery times, with the exception of the femoral heads.

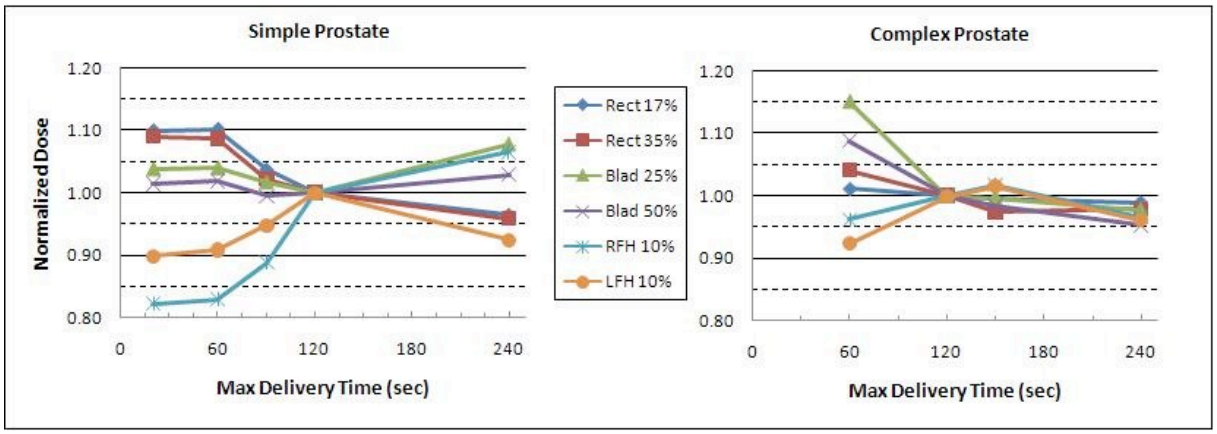

Figure 3-37. Normal tissue metrics for "Maximum Delivery Time" parameter for simple prostate and complex prostate cases. All doses normalized to dose values for the baseline trial (120 sec).

3.4 Monitor Units and Delivery Time

Two of the most advertised advantages of VMAT treatments are monitor unit and time efficiency. Table 3-22 shows the monitor units and estimated delivery time per fraction for each trial and each treatment geometry in this study. In general, the phantom case required the fewest MU and had the shortest fractional treatment times, while the the complex prostate case required the most MU and had the longest fractional treatment times. The phantom case also showed the least variation in MU and treatment times for any given parameter, while the complex prostate showed the most.

The original fixed-beam IMRT plan for the simple prostate patient required 719 MU/fraction. The estimated delivery time for this patient was between 8 and 11 minutes. The baseline VMAT plan (with comparable plan quality) required 34% fewer MU and 77% less time to deliver than the original IMRT plan for the simple prostate case. The complex prostate patient was originally treated with tomotherapy and required MU is unknown.

Table 3-22. MU and estimated delivery times for all parameters, trials, and treatment sites. All baseline trials are shown in bold.

Parameter	Trial	Phantom		Simple Prostate		Complex Prostate	
		MU	Delivery Time	MU	Delivery Time	MU	Delivery Time
Gantry speed variability	**yes**	**329**	**98**	**478**	**110**	**826**	**119**
	no	329	98	474	114	826	119
Maximum Gantry Speed	**6 deg/sec**	**329**	**98**	**478**	**110**	**826**	**119**
	4 deg/sec	329	97	479	110	805	117
	8 deg/sec	329	95	477	109	837	116
	12 deg/sec	329	95	476	109	845	117
Maximum Dose Rate	**Disc 600**	**329**	**98**	**478**	**110**	**826**	**119**
	Cont 600	329	98	474	113	812	119
	Disc 400	329	99	455	117	737	121
	Cont 400	329	97	461	120	705	120
	Disc 800	329	99	488	110	791	99
	Cont 800	329	97	482	106	789	106
Maximum MLC Leaf Speed	**2 cm/sec**	**329**	**98**	**478**	**110**	**826**	**119**
	3 cm/sec	329	98	469	112	763	115
	1 cm/sec	329	98	439	107	722	115
MLC size	**1 cm**	**329**	**98**	**478**	**110**	**826**	**119**
	0.5 cm	332	105	449	99	870	118
Maximum MU/degree	**100 MU/deg**	**329**	**98**	**478**	**110**	**826**	**119**
	1 MU/deg	329	98	473	107	826	119
Beam Energy	**6 MV**	**329**	**98**	**478**	**110**	**826**	**119**
	10 MV	279	112	407	113	855	118
	15 MV	266	98	387	107	760	115
Arc Length	60 deg	384	109	506	120	930	129
	120 deg	355	112	379	122	935	140
	180 deg	345	100	463	106	924	115
	270 deg	329	105	402	108	804	117
	360 deg	**329**	**98**	**478**	**110**	**826**	**119**
Collimator Angle	0 deg	331	97	**478**	**110**	**826**	**119**
	30 deg	331	107	432	106	737	119
	45 deg	336	104	442	114	772	127
	60 deg	334	98	402	113	841	118
	90 deg	**329**	**98**	399	122	756	119
Dose Grid Resolution	**0.4 cm**	**329**	**98**	**478**	**110**	**826**	**119**
	0.3 cm	334	120	506	113	--	--
	0.5 cm	329	97	458	110	832	121
Final Gantry spacing	**4 deg**	**329**	**98**	**478**	**110**	**826**	**119**
	2 deg	329	98	493	108	--	--
	3 deg	329	103	481	106	--	--
	6 deg	332	120	460	83	665	96
Maximum Delivery Time	**120 sec**	**329**	**98**	**478**	**110**	**826**	**119**
	60 sec	330	60	424	60	618	64
	240 sec	329	194	482	211	892	194

4 DISCUSSION

In this study, we varied several parameters independently for 3 treatment geometries of increasing complexity to determine their effect on resulting plan quality for VMAT treatment planning. We found that most parameters had a small effect (<0.02 variation from baseline values) on DHI and CI for both phantom and simple prostate cases and a larger effect (>0.02 variation from baseline values) on DHI and CI for the complex prostate case. Even though greater than 0.02 variation from baseline DHI and CI values was found for most parameters for the complex prostate case, the data was inconclusive of predictable trends for varying any parameters other than total arc length. Similarly, the normal tissue metrics showed less than 3% change for most parameters for the simple prostate case and greater than 3% change for the complex prostate case with few predictable trends.

We observed that in effect, one can use a wide variety of values for any set of parameters with very little change in the resulting plans for non-complex cases. In some instances, this is because parameters are subject to an override by Pinnacle (i.e. maximum delivery time, maximum gantry speed). We also speculate that because all parameters are optimized together, there are enough degrees of freedom built into VMAT optimization to compensate for any one parameter that would otherwise cause the optimization algorithm to struggle (i.e. maximum gantry speed, maximum MLC leaf speed). This was especially true when varying commissioning parameters for the two non-complex cases. For these reasons we have determined that for non-complex treatment sites, SmartArc optimization is largely user-input-independent and hardware independent, whereas complex treatment sites show a greater dependency on input parameter values.

4.1 Comparison to Previous Literature

Literature concerning how varying certain parameters affects the resulting plan quality is limited. Su *et al.* used DMPO optimization for fixed-beam IMRT treatments to study the effects of varying leaf width from 5mm to 1cm on resulting plan quality and accuracy (Su *et al*. 2007). They concluded that leaf width showed no significant difference in CI or DHI for head and neck, prostate, or spine geometries, but that there was slightly better dose accuracy for 1cm leaves. Our study showed similar results for CI and DHI; all but one PTV (PTV3 of the complex prostate case) had DHI changes of less than 2%, and the greatest difference in CI was only 3% for the complex prostate case. The issue of beam energy has also been studied previously for IMRT treatments. Pirzkall *et al*. showed that prostate IMRT treatments with less than 9 fields could result in dose increases in tissues distant to the target volume (i.e. near the skin surface) for lower energies (6MV), even though PTV and avoidance structure metrics were the same for 6, 10, and 18MV. Studies have also shown that with a greater number of fields (>9), the difference between dose distributions for different beam energies disappears (Pirzkall *et al.* 2002; Fox *et al.* 2008). We found that there was no identifiable trend for increasing beam energy of VMAT plans, but significant changes were seen in the DHI values of the complex prostate PTVs and the CI and normal tissue metrics for all treatment geometries. However, we speculate that the effects of beam energy may not translate directly from fixed-beam IMRT to VMAT treatment plans, as the beam shape modulation is more restricted for VMAT planning.

While previous studies focus on one or two parameters of interest, we conducted a systematic one dimensional examination of all the major VMAT parameters (commissioning and planning) for geometries of varying complexity. This allowed us to provide information comparing capabilities of different machines and different vendors. This study concludes that

two major differences between Varian and Elekta machines (MLC leaf width and continuously or discretely variable dose rates) are largely inconsequential.

4.2 Limitations and Future Work

There were several limitations to this study. First, only one parameter was varied at a time, while all the others were held fixed. Possible interdependencies between the parameters might have a larger effect on resulting plan quality if multiple parameters were changed simultaneously. For example, the beam shape modulation between control points depends on *both* the maximum MLC leaf speed and the maximum gantry speed. Varying several parameters at once to study their combined effects on resulting plan quality could be valuable future research. This could be done by randomly sampling a multi-dimensional complex space, as it would be impossible to vary all parameters systematically (over 800,000 possible combinations for the parameter values varied in this study).

In addition to varying multiple parameters together, it would be beneficial to investigate how changing parameters effects plan *accuracy*, not just resulting plan *quality*. While this study thoroughly investigated how each parameter effects the resulting DHI, CI, and dose metrics calculated internally by the treatment planning system, it remains unknown how well the calculated doses match what is actually being delivered by the treatment machine.

4.3 Clinical Relevance

Since the time this study was done, a clinical version (9.0) of Pinnacle including the SmartArc module has been released, improving upon the research version (8.1y) by including double arc capabilities and allowing the jaws to move with the MLC to provide additional collimation. To check the clinical validity of the plans created using the research version, test plans for the complex prostate case were run on Pinnacle 9.0. A new baseline plan was created

Table 4-1. DHI and CI results for varying final gantry spacing on the research (8.1y) and clinical (9.0) versions of Pinnacle.

Version	Trial	DHI (PTV1)	DHI (PTV 2)	DHI (PTV 3)	DHI (PTV 4)	CI
8.1y	4 deg	0.16	0.13	0.61	0.74	0.79
	6 deg	0.19	0.11	0.63	0.75	0.67
9.0	4 deg	0.15	0.11	0.57	0.77	0.83
	6 deg	0.18	0.12	0.61	0.79	0.83

on Pinnacle 9.0 that provided dose values equal to or better than those provided by the 8.1y baseline plan. Trials were run for 4 degree and 6 degree final gantry spacing using Pinnacle 9.0, and compared to the 4 degree and 6 degree trials run on Pinnacle 8.1y. The results for DHI and CI for both versions of Pinnacle are shown in Table 4-1. The change in DHI from 4 degree final gantry spacing to 6 degree final gantry spacing is similar for the research and clinical versions of Pinnacle. The CI showed a change for the research version, but not for the clinical version. The CI also performed better for the clinical version of Pinnacle.

4.4 Optimization Noise

We considered a 0.02 variation in DHI or CI values to be a significant change, and a 3% difference in normal tissue metrics to be a significant change. These increments were based on what we determined to be **clinically** significant changes. In other words, changes of this magnitude would make one plan favorable to another in a clinical setting. In order to assess a **statistically** significant difference, it was necessary to determine the uncertainty in the optimization algorithm, or "optimization noise." To do this, very small changes were made to the baseline plans for each treatment geometry, either to the original optimization goals or to the dose grid resolution. These slightly modified plans were re-optimized and the doses re-computed. The trials for determining optimization noise by modifying an optimization goal are described in Table 4-2. Dose grid resolution was also slightly modified to determine optimization noise and dose calculation uncertainty. In trials 6 and 7 for the phantom, simple

Table 4-2. Description of trials used to determine optimization noise by modifying an optimization goal.

Geometry	Trial	Weight	ROI	Type	Original Goal	New Goal
Phantom	Trial 2	10	PTV	Max Dose	205	204
	Trial 3	10	PTV	Max Dose	205	206
Simple Prostate	Trial 2	45	PTV	Min DVH	7600	7601
	Trial 3	45	PTV	Min DVH	7600	7599
Complex Prostate	Trial 2	25	4620 only	Uniform	4620	4621
	Trial 3	25	4620 only	Uniform	4620	4619
	Trial 4	100	PTV 1	Uniform	7800	7801
	Trial 5	100	PTV 1	Uniform	7800	7799

Table 4-3. Description of trials used to determine optimization noise and dose calculation uncertainty by modifying the dose grid resolution.

Geometry	Trial	Re-optimization?	Original Dose Grid Resolution (cm)	New Dose Grid Resolution (cm)
Phantom, Simple Prostate, Complex Prostate	Trial 6	yes	0.400	0.401
	Trial 7	yes	0.400	0.399
	Trial 8	no	0.400	0.401
	Trial 9	no	0.400	0.399

prostate, and complex prostate cases, the dose grid resolution was changed to 0.401cm and 0.399cm, respectively, from the original resolution of 0.400cm. After the dose grid resolution was modified for trials 6 and 7, plans were re-optimized and the dose was re-computed. The dose grid resolution for trials 8 and 9 was modified similarly to trials 6 and 7, but the plans were not re-optimized – only the dose was recomputed. Trials 6 and 7 are meant to show a combined effect of optimization noise and dose calculation uncertainty, while trials 8 and 9 only show the dose calculation uncertainty. Table 4-3 describes trials 6 through 9.

Results for determining optimization noise are shown in Table 4-4. Metrics used in the study for all PTVs (DHI and CI) were normalized to the baseline values. The table shows the difference between the values for DHI and CI for each trial and the baseline DHI and CI values (ΔDHI and ΔCI). For trials 2-5 for all treatment geometries, the differences in DHI and CI were

less than 0.002, the criteria for clinical significance. For trials 6 and 7 (re-optimization and re-calculation of dose), the greatest difference in DHI was 0.04, and the greatest difference in CI was 0.03. The average of all numbers in trials 6 and 7 was 0.013, which is less than the value for clinical significance. DHI and CI values for trials 8 and 9 (no re-optimization) showed no difference from the baseline DHI and CI values. Though there is undoubtedly both optimization noise and dose calculation uncertainty in the treatment planning system, we determined that the values for optimization and dose calculation uncertainty are less than our criteria for clinical significance.

Table 4-4. Results for optimization noise. Values represent the change in DHI and CI values from the baseline values for each trial.

Trial	Phantom		Simple Prostate		Complex Prostate				
					PTV1		PTV2	PTV3	PTV4
	ΔDHI	ΔCI	ΔDHI	ΔCI	ΔDHI	ΔCI	ΔDHI	ΔDHI	ΔDHI
Baseline	0.00	0.00	0.00	0.00	0.0	0.0	0.0	0.0	0.0
2	0.00	**0.01**	0.00	0.00	0.00	0.00	0.00	0.00	0.00
3	0.00	0.00	0.00	0.00	**0.01**	0.00	**0.01**	0.00	0.00
4	--	--	--	--	**0.01**	**0.02**	0.00	**0.02**	0.00
5	--	--	--	--	0.00	**0.02**	0.00	0.00	0.00
6	0.00	**0.01**	**0.02**	**0.03**	0.00	**0.01**	**0.03**	**0.01**	**0.01**
7	0.00	0.00	**0.01**	**0.01**	**0.01**	**0.01**	**0.04**	**0.02**	**0.02**
8	0.00	0.00	0.00	0.00	0.00	0.00	0.00	0.00	0.00
9	0.00	0.00	0.00	0.00	0.00	0.00	0.00	0.00	0.00

5 CONCLUSIONS

In conclusion, we used the Pinnacle SmartArc treatment planning module to systematically examine the effects of varying parameters on resulting VMAT treatment plans. The study was intentionally robust, allowing us to answer our initial hypothesis in a clinically relevant way. We were able to create better than ±3% dose homogeneity in the PTV of a phantom, and better than ±5% dose homogeneity in the PTV of a simple prostate patient for a wide range of input parameter values, while keeping treatment times better than half of corresponding fixed-beam IMRT plans. We were unable to achieve better than ±5% dose homogeneity in the primary PTV of a complex prostate patient, though the baseline plan we created was clinically acceptable and treatment times were still less than half of standard fixed-beam IMRT treatments. We found that SmartArc is largely user-independent and machine hardware-independent for non-complex treatment geometries, but significant changes (>0.02 variation from baseline values for DHI and CI and >3% variation from baseline values for normal tissue metrics) in plan quality can be seen when varying parameters for complex geometries. This is useful information for centers when implementing protocols for VMAT treatment planning or investigating which vendor provides the most compatible machine hardware to their facility.

REFERENCES

Bortfeld T and Webb S 2009 Single-Arc IMRT? Phys Med Biol 54 N9-20

Bzdusek K, Friberger H, Eriksson K, Hardenmark B, Robinson D and Kaus M 2009 Development and evaluation of an efficient approach to volumetric arc therapy planning Med Phys 36 2328-39

Cao D, Holmes T W, Afghan M K and Shepard D M 2007 Comparison of plan quality provided by intensity-modulated arc therapy and helical tomotherapy Int J Radiat Oncol Biol Phys 69 240-50

Earl M A, Shepard D M, Naqvi S, Li X A and Yu C X 2003 Inverse planning for intensity-modulated arc therapy using direct aperture optimization Phys Med Biol 48 1075-89

Friberger H 2009 SmartArc in Pinnacle 9: A description of the algorithm RaySearch Laboratories

Fox C, Romeijn H E, Lynch B, Men C, Aleman D and Dempsey J 2008 Comparative analysis of 60Co intensity-modulated radiation therapy Phys Med Biol 53 3175-88

Khan F M 2003 The physics of radiation therapy (Philadelphia: Lippincott Williams & Wilkins)

Lee T K, Rosen, II, Gibbons J P, Fields R S and Hogstrom K R 2008 Helical tomotherapy for parotid gland tumors Int J Radiat Oncol Biol Phys 70 883-91

Mackie T R, Holmes T, Swerdloff S, Reckwerdt P, Deasy J O, Yang J, Paliwal B and Kinsella T 1993 Tomotherapy: a new concept for the delivery of dynamic conformal radiotherapy Med Phys 20 1709-19

Otto K 2008 Volumetric modulated arc therapy: IMRT in a single gantry arc Med Phys 35 310-7

Palma D, Vollans E, James K, Nakano S, Moiseenko V, Shaffer R, McKenzie M, Morris J and Otto K 2008 Volumetric modulated arc therapy for delivery of prostate radiotherapy: comparison with intensity-modulated radiotherapy and three-dimensional conformal radiotherapy Int J Radiat Oncol Biol Phys 72 996-1001

Pirzkall A, Carol M P, Pickett B, Xia P, Roach M 3rd and Verhey L J 2002 The effect of beam energy and number of fields on photon-based IMRT for deep-seated targets Int J Radiat Oncol Biol Phys 53 434-42

Pollack A, Price R, Dong L, Feigenberg S and Horwitz E M 2005 Intact Prostate Cancer: Overview Intensity Modulated Radiation Therapy: a clinical perspective eds. Mundt A and Roeske J 436-45

Reft C S, Runkel-Muller R and Myrianthopoulos L 2006 In vivo and phantom measurements of the secondary photon and neutron doses for prostate patients undergoing 18 MV IMRT Med Phys 33 3734-42

Shah A P, Chen S S, Strauss J B, Kirk M C, Coleman J L, Coon A B, Miller C and Dickler A 2009 A Dosimetric Analysis Comparing Treatment of Low-Risk Prostate Cancer With TomoTherapy Versus Static Field Intensity Modulated Radiation Therapy Am J Clin Oncol

Shaffer R, Morris W J, Moiseenko V, Welsh M, Crumley C, Nakano S, Schmuland M, Pickles T, and Otto K 2009 Volumetric Modulated Arc Therapy and Conventional Intensity-modulated Radiotherapy for Simultaneous Maximal Intraprostatic Boost: a Planning Comparison Study Clin Oncol

Staffurth J 2010 A review of the clinical evidence for intensity-modulated radiotherapy Clin Oncol 22 643-57

Su Z, Kim S, Liu C and Palta J 2006 Is Dosimetric Effect of Leaf Width of MLC Clinically Significant in IMRT IFMBE Proceedings eds. Kim S and Suh T S 14 1766-69

Svensson R, Kallman P and Brahme A 1994 An analytical solution for the dynamic control of multileaf collimators Phys Med Biol 39 37-61

Verbakel W F, Cuijpers J P, Hoffmans D, Bieker M, Slotman B J and Senan S 2009 Volumetric intensity-modulated arc therapy vs. conventional IMRT in head-and-neck cancer: a comparative planning and dosimetric study Int J Radiat Oncol Biol Phys 74 252-9

Webb S and McQuaid D 2009 Some considerations concerning volume-modulated arc therapy: a stepping stone towards a general theory Phys Med Biol 54 4345-60

Wu Y, Yan D, Sharpe M B, Miller B and Wong J W 2001 Implementing multiple static field delivery for intensity modulated beams Med Phys 28 2188-97

Yang J N, Mackie T R, Reckwerdt P, Deasy J O and Thomadsen B R 1997 An investigation of tomotherapy beam delivery Med Phys 24 425-36

Yu C X 1995 Intensity-modulated arc therapy with dynamic multileaf collimation: an alternative to tomotherapy Phys Med Biol 40 1435-49

Zhang P, Happersett L, Hunt M, Jackson A, Zelefsky M and Mageras G 2009 Volumetric modulated arc therapy: planning and evaluation for prostate cancer cases Int J Radiat Oncol Biol Phys

VITA

The daughter of Tom Scott Talbert, Jr. and Elizabeth Kay Turner Talbert, Catharine Elizabeth Talbert grew up in Wichita Falls, Texas. After graduating 9th in her class of 389 at Rider High School in 2003, she went to Texas Christian University in Fort Worth, Texas, where she studied mathematics and modern dance. In the fall of 2004, she transferred to Austin College in Sherman, Texas. She majored in physics, minored in philosophy and received a Bachelor of Arts degree in May, 2007. She entered the Medical Physics and Health Physics Program at Louisiana State University in the fall of 2007 and will receive the Master of Science degree in medical physics in 2010. She married Michael Haveman of Bloomington, Minnesota, in April 2010.